Cell Death & Differentiation (2021) 28:1512–1531
https://doi.org/10.1038/s41418-020-00683-x

Cell Death & Differentiation

ARTICLE

# BCL(X)L and BCL2 increase the metabolic fitness of breast cancer cells: a single-cell imaging study

Federico Lucantoni[1,2,5] · Manuela Salvucci[1,2] · Heiko Düssmann[1,2] · Andreas U. Lindner[1,2] · Diether Lambrechts[3,4] · Jochen H. M. Prehn[1,2]

Received: 4 March 2020 / Revised: 9 November 2020 / Accepted: 11 November 2020 / Published online: 16 December 2020


## Abstract

The BCL2 family of proteins regulate apoptosis by controlling mitochondrial outer membrane permeability. However, the effects on mitochondrial structure and bioenergetics have also been reported. Here we comprehensively characterized the effects of BCL2 and BCL(X)L on cellular energetics in MCF7 breast cancer cells using time-lapse confocal single-cell imaging and mitochondrial and cytosolic FRET reporters. We found that BCL2 and BCL(X)L increase the metabolic robustness of MCF7 cells, and that this was associated with increased mitochondrial NAD(P)H and ATP levels. Experiments with the $F_1F_0$ synthase inhibitor oligomycin demonstrated that BCL2 and in particular BCL(X)L, while not affecting ATP synthase activity, more efficiently coupled the mitochondrial proton motive force with ATP production. This metabolic advantage was associated with an increased resistance to nutrient deprivation and enhanced clonogenic survival in response to metabolic stress, in the absence of profound effects on cell death. Our data suggest that a primary function of BCL(X)L and BCL2 overexpression in tumor cells is to increase their resistance to metabolic stress in the tumor microenvironment, independent of cell death signaling.

## Introduction

BCL2 family members regulate the intrinsic apoptosis pathway by controlling the process of mitochondrial outer membrane permeabilization (MOMP) [1]. Apart from this function, BCL2 proteins also regulate mitochondrial fusion and fission [2–5]. This process is important for mitochondrial quality control, but also regulates mitochondrial bioenergetics [6]. BCL2 proteins may also control mitochondrial metabolism directly. BCL2 and BAX regulate the activity of the mitochondrial adenine nucleotide translocator [7]. BCL(X)L preserves the physiological conformation of the voltage-dependent anion channel (VDAC) and promotes exchange of metabolites [8]. In neurons, a pool of BCL(X)L has been found to localize in the inner mitochondrial membrane (IMM) and to interact with $F_1F_0$ ATP synthase, increasing its enzymatic activity and stabilizing mitochondrial membrane potential ($\Delta\Psi_m$) [9, 10]. A similar function was attributed to a truncated form of MCL1 that localizes to the matrix [11].

A comprehensive characterization of the effects of BCL2 and BCL(X)L on mitochondrial bioenergetics at the single-cell level and its relation to the process of MOMP has rarely been performed. It is important to dissect these events at this level, as cell death signaling may affect metabolism and vice versa [12, 13]. The effects of BCL2 family proteins on bioenergetics may be particularly important in cancer cells, which undergo periods of metabolic stress, and indeed often accumulate extraordinary high levels of BCL2 and BCL(X)L as seen in

Edited by C. Borner

**Supplementary information** The online version of this article (https://doi.org/10.1038/s41418-020-00683-x) contains supplementary material, which is available to authorized users.

✉ Jochen H. M. Prehn
jprehn@rcsi.ie

[1] Department of Physiology & Medical Physics, Royal College of Surgeons in Ireland, Dublin 2, Ireland

[2] Centre for System Medicine, Royal College of Surgeons in Ireland, Dublin 2, Ireland

[3] VIB Centre for Cancer Biology, Leuven, Belgium

[4] Laboratory of Translational Genetics, Department of Human Genetics, KU Leuven, Leuven, Belgium

[5] Present address: Departamento de Farmacología, Universitat de València; FISABIO (Fundación para el Fomento de la Investigación Sanitaria y Biomédica de la Comunidad Valenciana), Valencia, Spain

breast cancer [14–16]. Here, we aimed to comprehensively characterize the effects of BCL2 and BCL(X)L on cellular energetics in breast cancer cells using time-lapse single-cell imaging and mitochondrial/cytosolic ATP FRET reporters.

## Results

### Characterization of BCL2- and BCL(X)L-overexpressing ER$^+$ MCF7 breast cancer cells

We assessed absolute BCL2 protein levels in previously characterized MCF7 cells stably overexpressing BCL2 or BCL(X)L [17–19], using BCL2 quantitative western blotting [20] (Fig. 1a and b). MCF7-pSFFV (control) cells showed a higher BCL2 concentration over BCL(X)L and MCL1 (Fig. 1a and b). In MCF7–BCL2 cells, BCL2 was present at a concentration of 5.59 µM, while MCF7–BCL(X)L had levels comparable to MCF7-pSFFV cells (0.35 µM). BCL(X)L reached a concentration of 3.5 µM in MCF7–BCL(X)L (Fig. 1b). MCL1, BAX and BAK levels were similar in the three cell lines (Supplementary Fig. 1A and B). Thus, high BCL2 or BCL(X)L levels were observed in the respective overexpressing cell lines, with little compensatory alterations in other BCL2 proteins.

Next, we analyzed the subcellular localization of BCL2 and BCL(X)L in the respective overexpressing cells, through immunofluorescence. Both BCL2 and BCL(X)L antibodies co-localized with MitoTracker Red CMXRos, while no signal was detected in the nucleus (Fig. 1c). BCL(X)L cells displayed slightly different sub-localization pattern when compared to BCL2 cells, as previously reported in the same cell lines, by Antonietti et al. [17, 21].

We also tested whether BCL2- and BCL(X)L-overexpressing MCF7 possessed enhanced survival rates following exposure to staurosporine (STS, 2 µM) or cisplatin (40 µM) through flow cytometry. MCF7-pSSFV were susceptible to both treatments, while BCL2- and BCL(X)L-overexpressing cell lines were less sensitive (Fig. 1d and e).

### BCL2- and BCL(X)L-expressing cells produce similar amounts of mitochondrial ATP by employing less mitochondrial NAD(P)H

We transfected cells with a plasmid encoding a mitochondrial targeted ATP FRET probe [22], which was multiplexed with the $\Delta\Psi_m$ sensitive dye TMRM, to measure alterations in mitochondrial ATP levels simultaneously with $\Delta\Psi_m$ depolarization or hyperpolarization [23, 24]. To investigate the effects of BCL2 and BCL(X)L on mitochondrial bioenergetics without contribution from glycolysis, cells were starved for 3 h and then fueled with the mitochondrial substrate pyruvate. Cells were imaged with a laser-scanning confocal microscope every minute (Supplementary Fig. 2A). Baseline values during starvation were recorded for the first 20 min; then 2 mM pyruvate was added, and single-cell kinetics were followed for another 20 min. Finally, ATP synthase inhibitor oligomycin was used to block the $F_0$ subunit of the ATP synthase.

Pyruvate addition activated mitochondrial ATP production, observed through an increase in the normalized FRET/CFP ratio in all three cell lines (Fig. 2a). Following oligomycin, mitochondrial ATP dropped as a result of ATP synthase inhibition (Fig. 2a). $\Delta\Psi_m$ increased during pyruvate exposure due to electron transport chain (ETC) activity and further increased after oligomycin addition, due to proton motive force not being used for ATP production (Fig. 2a). We compared the absolute FRET/CFP ratio of the three different MCF7 clones, which is more indicative of actual mitochondrial ATP (Fig. 2b). Baseline and post-pyruvate addition of mitochondrial ATP levels were lower in BCL2 cells when compared to MCF7-pSFFV and BCL(X)L cells. Following oligomycin, ATP levels were similar in all cell lines (Fig. 2b). Interestingly, a lower absolute TMRM fluorescence was recorded for BCL2- and BCL(X)L-overexpressing cells at baseline (Fig. 2d). Furthermore, BCL(X)L cells showed a significantly higher $\Delta\Psi_m$ following oligomycin addition, when compared to the other cells (Fig. 2a and c).

Using similar treatment protocol, we next measured NAD(P)H kinetics (Supplementary Fig. 2B). An increase in NAD(P)H fluorescence was measured when pyruvate was added to the experimental buffer (Fig. 2e). Quantification of NAD(P)H levels in the different cells revealed that during starvation and after pyruvate addition, BCL2 and BCL(X)L cells accumulated higher NAD(P)H levels (Fig. 2f). Despite lower NAD(P)H levels, MCF7-pSFFV cells exhibited higher NAD(P)H production kinetics following pyruvate (Fig. 2e). Slope analyses for pyruvate addition revealed that both MCF7–BCL2 and BCL(X)L displayed slower NAD(P)H production rates when compared to MCF7-pSFFV (Fig. 2g). Next, we calculated the NAD(P)H/ATP ratio, by dividing NAD(P)H absolute fluorescence to FRET/CFP absolute ratio. We found that in all conditions, MCF7–BCL2 and BCL(X)L cells accumulated a higher ratio when compared to MCF7-pSFFV cells (Fig. 2h). This suggested that BCL2- and BCL(X)L-overexpressing clones produce similar amount of mitochondrial ATP, by employing significantly less mitochondrial NAD(P)H.

### BCL2- and BCL(X)L-overexpressing cell lines couple the mitochondrial proton motive force with ATP production in a more efficient way

We next explored whether BCL2 and BCL(X)L were acting on $F_1F_0$ ATP synthase to enhance mitochondrial energetics

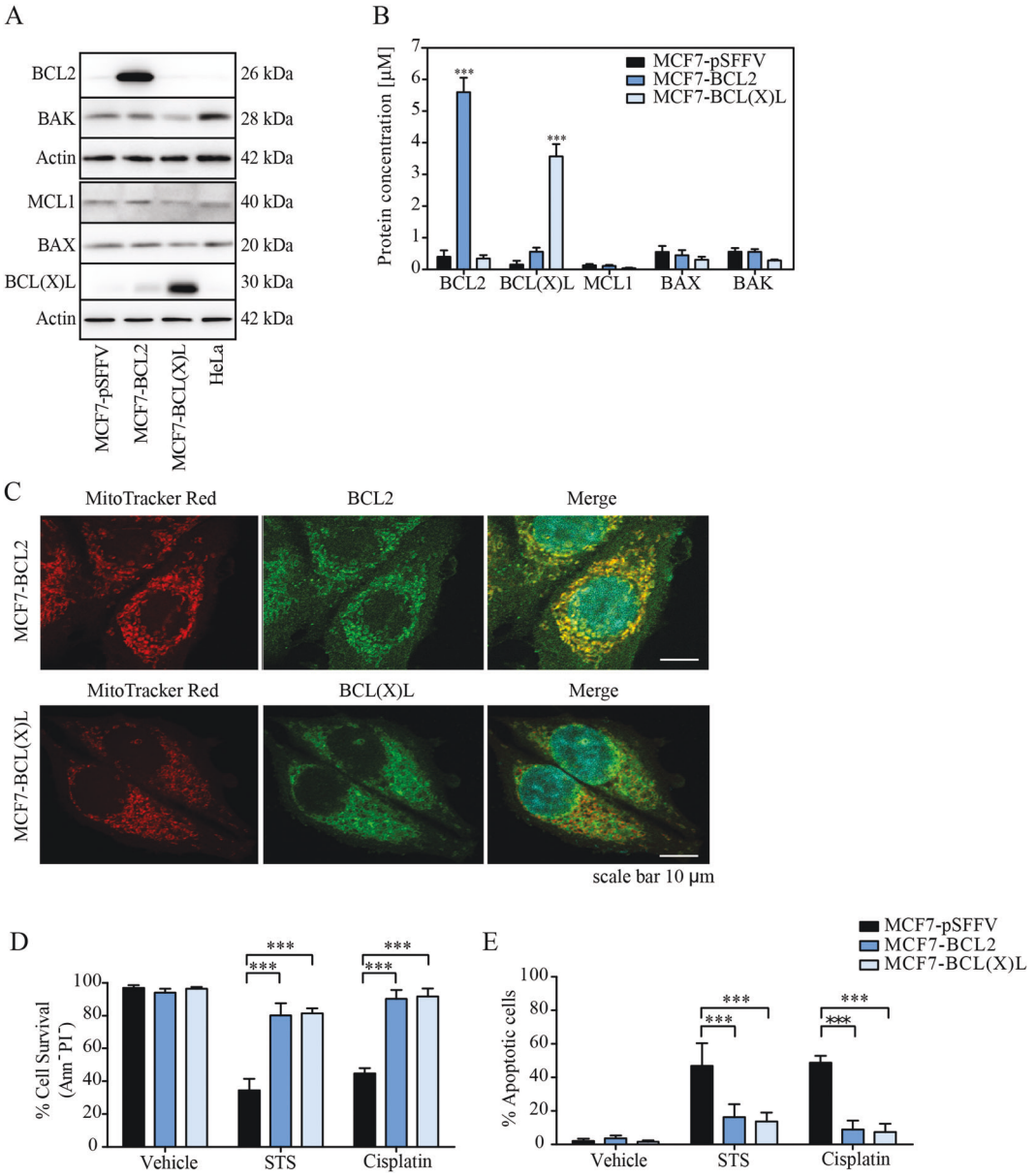


**Fig. 1 Characterization of MCF7 clones. a** Representative WB for MCF7 cell lines. Cells were lysed and analyzed by immunoblotting to detect levels of two pro-apoptotic proteins, BAX and BAK, and three anti-apoptotic proteins, BCL2, BCL(X)L and MCL1. Actin was used as loading control to normalize protein concentration values post densitometry, and HeLa cell line lysates were used for absolute quantification. **b** Expression levels for BCL2 proteins as determined by comparing densitometric signals and considering absolute quantification levels in HeLa cells. Data represent mean ± SD from $n = 3$ independent experiments and quantifications were analyzed by two-way ANOVA with Tukey post test (* indicates a $p$ value < 0.5, ** indicates a $p$ value < 0.01, *** indicates a $p$ value < 0.001). **c** Immunofluorescence staining showing localization of BCL2 and BCL(X)L, respectively. MCF7–BCL2 and BCL(X)L-overexpressing cells were fixed with paraformaldehyde (4% PFA) and permeabilized with a solution of 95% ethanol and 5% glacial acetic acid. DAPI was used to visualize nuclei, while MitoTracker Red CMXRos was used to stain mitochondria. Images are representative of immunofluorescence performed on $n = 3$ independent cultures. **d** Percentages of surviving cells (Annexin V-/PI fraction) following 24 h of control, STS (2 µM) or cisplatin (40 µM) treatment. **e** Percentages of apoptotic cells (sum of Annexin V+ /PI− and Annexin V+ /PI+ fractions) post treatments. Significance was assessed with a two-way ANOVA and Tukey post test (* indicates a $p$ value < 0.05, ** indicates a $p$ value < 0.01, *** indicates a $p$ value < 0.001). Column represents mean ± SD for $n = 3$ experiments.

of breast cancer cells, by performing an oligomycin titration. Cells, transiently transfected with mitochondrial ATeam probe, were placed in KB with 2 mM pyruvate; after 20 min of baseline, we applied 1 nM, 10 nM and 100 nM oligomycin, every 20 min (Supplementary Fig. 3). These concentrations were chosen in order to avoid saturation of ATP synthase. ATP production decreased after addition of 1 nM oligomycin in all cell lines, while TMRM

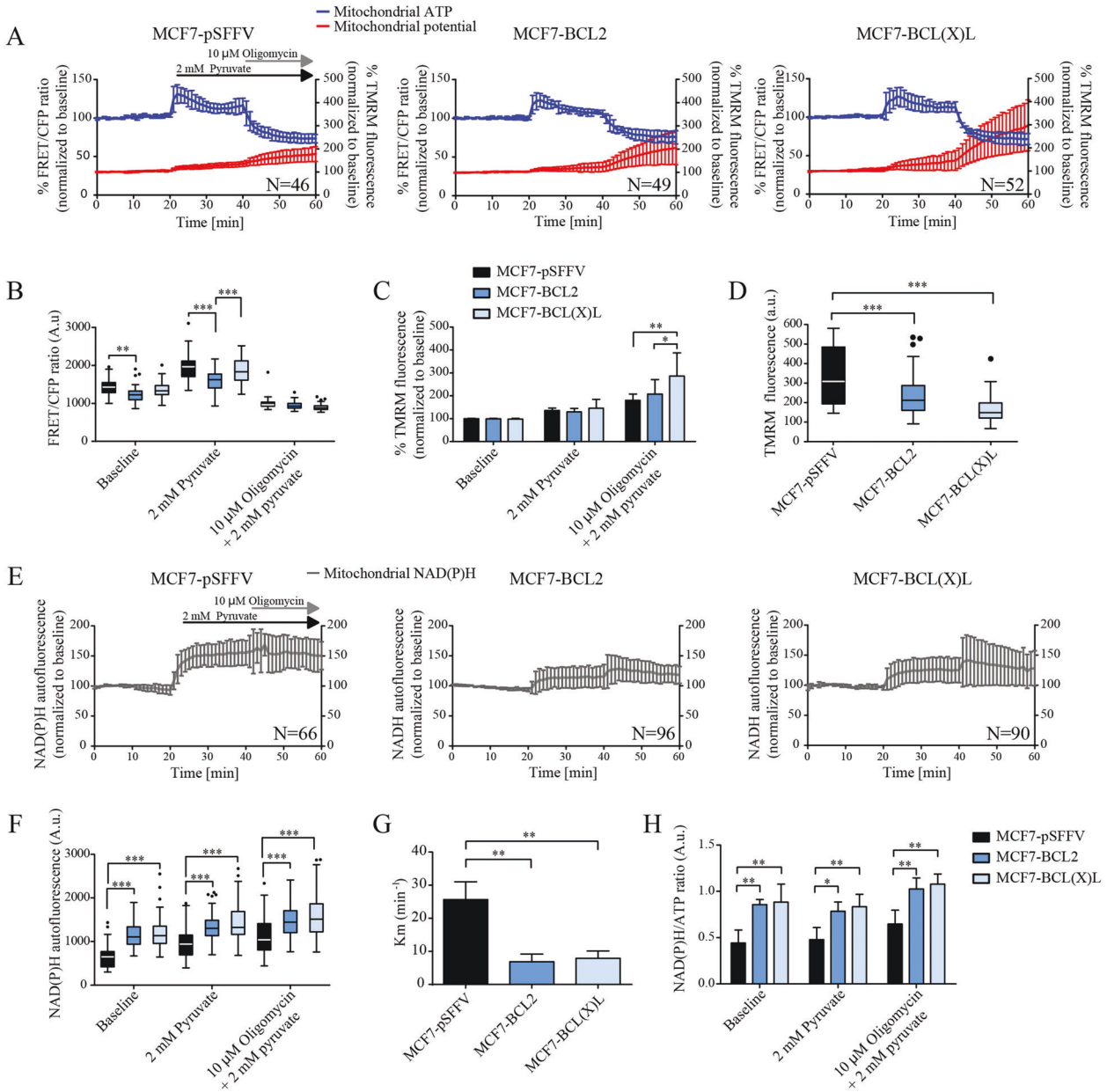


**Fig. 2 MCF7–BCL2 and BCL(X)L clones produce similar amounts of mitochondrial ATP by producing/consuming less NAD(P)H, when compared to MCF7-pSFFV cells. a** Representative traces of mitochondrial ATP signal and mitochondrial membrane potential. FRET/CFP ratio kinetics and TMRM fluorescence were monitored simultaneously in all MCF7 clones. Cells were starved for 3 h; after that, the baseline was recorded for 20 min and 2 mM sodium pyruvate was added into the medium. Following 20 min of treatment, 10 µM oligomycin was supplemented for the last 20 min. All data represent mean ± SD from $n = 4$–5 independent experiments and both signals are normalized to the baseline levels (each cell line normalized to its own baseline). **b** The absolute FRET/CFP ratio was analyzed by taking into account the maximal value reached by the probe after pyruvate addition and minimal value after oligomycin treatment. Box and whiskers represent single-cell values from all experiments. **c** TMRM-intensity values, normalized to the baseline levels from TMRM kinetics, were analyzed by taking into account the maximal value reached following each treatment. **d** TMRM fluorescence absolute values obtained from baseline. Box and whiskers represent single-cell values from all experiments. All values were analyzed by two-way ANOVA with Tukey post test (* indicates a $p$ value < 0.05, ** indicates a $p$ value < 0.01, *** indicates a $p$ value < 0.001). **e** Representative traces of mitochondrial NAD(P)H signal. NAD(P)H autofluorescence was monitored in all MCF7 clones, by following similar experimental protocol as above. All data represent mean ± SD from $n = 3$ independent experiments and signals are normalized to the baseline levels (each cell line normalized to its own baseline). **f** The absolute NAD(P)H fluorescence was analyzed by taking into account the maximal autofluorescence value reached after treatments. Box and whiskers represent single-cell values from all experiments. **g** NAD(P)H curve fitting for pyruvate addition was calculated using a fit function in GraphPad Prism. **h** NAD(P)H/ATP ratio, calculated by dividing NAD(P)H absolute fluorescence to absolute mitoAteam FRET/CFP ratio. All values were analyzed by two-way ANOVA with Tukey post test (* indicates a $p$ value < 0.05, ** indicates a $p$ value < 0.01, *** indicates a $p$ value < 0.001).

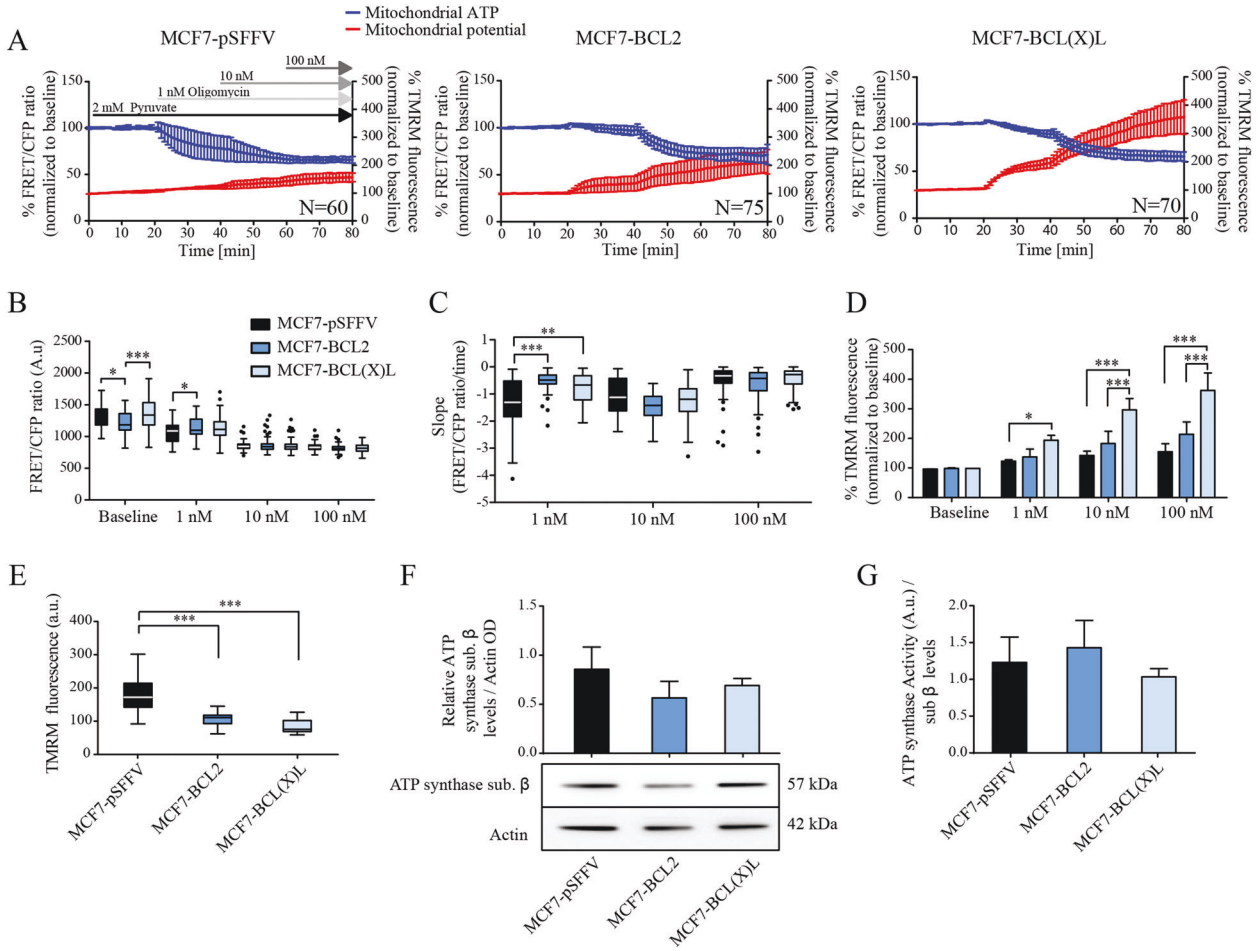


**Fig. 3 BCL2 and BCL(X)L cells maintain higher mitochondrial ATP after oligomycin titration. a** Representative traces of mitochondrial ATP signal and mitochondrial membrane potential. FRET/CFP ratio kinetics and TMRM fluorescence were monitored simultaneously in all MCF7 clones. Cells were placed in KB with 2 mM pyruvate; baseline was recorded for 20 min and oligomycin titration started by adding 1 nM, 10 nM and 100 nM of the drug with an interval of 20 min for each concentration. All data represent mean±SD from $n = 3$ independent experiments and both signals are normalized to the baseline levels (each cell line normalized to its own baseline). **b** The absolute FRET/CFP ratio was analyzed by taking into account the minimal value reached by the probe after each addition. **c** Slope values of oligomycin titration were assessed by dividing the ΔFRET/CFP ratio to the Δtime (time offset–time onset). Box and whiskers represent single-cell values from all experiments. **d** TMRM-intensity values normalized to the baseline levels from TMRM kinetics were analyzed by taking into account the maximal value reached after each treatment. All values were analyzed by two-way ANOVA with Tukey post test (* indicates a $p$ value < 0.05, ** indicates a p- value < 0.01, *** indicates a $p$ value < 0.001). **e** TMRM fluorescence absolute values obtained from baseline. **f** Protein levels for ATP synthase subunit β in MCF7 clones were obtained from cell lysates and normalized to actin. **g** A commercially available kit from Abcam was used after isolation of mitochondrial fraction from MCF7 cell lines, to calculate the activity of ATP synthase. In order to account for protein concentration, the activity was normalized to ATP synthase subunit β. All data represent mean ± SD from 3 independent experiments. All values were analyzed by one-way ANOVA with Tukey post test.

signal indicated increased $\Delta\Psi_m$ (Fig. 3a). Analysis of FRET/CFP ratios revealed that both MCF7–BCL2 and MCF7–BCL(X)L possessed higher ATP production following 1 nM oligomycin treatment compared to control cells. No changes were observed after 10 nM and 100 nM oligomycin addition, as the enzyme was likely saturated (Fig. 3b). Of note, an increased TMRM intensity was recorded in response to oligomycin for MCF7–BCL(X)L cells, compared to control cells (Fig. 3a and d). Kinetics analysis revealed higher slope values (see Materials and methods, time-lapse imaging section) for BCL2 and BCL(X)L clones after 1 nM oligomycin treatment (Fig. 3c), indicating slower ATP consumption (since larger negative slope values indicate a faster descent of the kinetic curve).

Next, we determined ATP synthase β-subunit protein levels by WB, as it was previously shown that BCL(X)L can establish an interaction with this subunit [9]. As shown in Fig. 3f no significant difference was detected. We determined the enzymatic activity of immunocaptured ATP synthase from isolated mitochondria by monitoring the oxidation reaction of NAD(P)H to NAD +. Again, no difference was observed (Fig. 3g). Moreover, we analyzed the

effect of the proton uncoupler FCCP on cytosolic ATP levels in pyruvate. We observed that BCL2- and BCL(X)L-overexpressing cells maintained higher cytosolic ATP levels after FCCP treatment (Supplementary Fig. 4). Collectively, these data suggested that BCL2- and BCL(X)L-overexpressing cancer cells possessed higher rates of proton motive force coupling, with little alterations in ATP synthase activity.

## BCL2- and BCL(X)L-overexpressing cells maintain higher cytosolic ATP levels during starvation and exhibit higher clonogenic potential during nutrient deprivation

To determine whether these mitochondrial alterations in BCL2 and BCL(X)L cells precipitated in survival/growth advantage during metabolic stress, we subjected MCF7 clones to nutrient depletion. As starvation has an impact on the cytosolic ATP kinetics, and we wanted to analyze the ability of BCL2 and BCL(X)L to rescue cell functions by maintaining cytosolic ATP levels, we here used the cytoplasmic version of the ATeam construct [22]. Cells were placed in KB with no nutrient, and cytosolic ATP levels measured over 24 h (Supplementary Fig. 5A). As shown in Fig. 4a, ATP kinetics decreased during the time course. Five millimolar glucose partially rescued ATP production due to glycolysis activation (Fig. 4a). $\Delta\Psi_m$ measured at the same time showed a small initial increase during the first 2–4 h, followed by a small decrease (Supplementary Fig. 5B). Measurement of the FRET/CFP ratio revealed lower baseline values for MCF7–BCL(X)L compared to pSFFV and BCL2 cells (Fig. 4b). From 12 h until the end of the experiment, both BCL2- and BCL(X)L-overexpressing cells maintained higher ATP levels compared to control cells (Fig. 4b). Kinetic analysis of ATP consumption highlighted higher slope values for MCF7–BCL2 and BCL(X)L compared to pSFFV cells, from 6 to 20 h after nutrient removal (Fig. 4c), suggesting slower ATP loss. TMRM levels were higher for BCL(X)L cells after 2, 6 and 18 h of starvation compared to the other cells (Supplementary Fig. 5B).

We next performed clonogenic assay under identical conditions as above. When cells were cultured in full RPMI medium (NT), BCL(X)L and BCL2 cells revealed a higher capacity to grow colonies over 7 days compared to MCF7-pSFFV (Fig. 4d and e). Similarly, in the starvation group [cells placed in SILAC (stable isotope labeling with amino acids in cell culture) medium with the addition of dialyzed fetal bovine serum, without glutamine or glucose] for 24 h and then switched to RPMI medium for 7 days, both BCL2- and BCL(X)L-overexpressing cells showed an increased clonogenic potential (Fig. 4d and e). Similar results were observed when the cells were grown in medium with 5 mM glucose (SILAC medium without glutamine and supplemented with 5 mM glucose). We also measured the levels of Annexin V-/PI-negative cells by flow cytometry. A survival of 90–100% was observed in all conditions and cell lines (Fig. 4f). Therefore, BCL2- and BCL(X)L-overexpressing cells possessed higher clonogenic potential during metabolic stress, both during nutrient starvation and in low-glucose media, and this effect was not accompanied by significant cell death induction (Fig. 4e and f).

## BCL2 and BCL(X)L cells possess increased mitochondrial respiration during hypoxia

Next, we investigated the potential role for BCL2 proteins in ATP consumption during hypoxia. First, we employed sodium azide and measured the levels of cytosolic ATP (using the cytosolic version of the ATeam construct, as we again aimed to analyze the ability of BCL2 and BCL(X)L to rescue cell functions by maintaining cytosolic ATP levels) when cells were fueled with pyruvate (Supplementary Fig. 6). After sodium azide treatment, a decrease in ATP production was observed in all cell lines (Fig. 5a), as this prevents cytochrome *c* oxidase from using $O_2$. In parallel, the TMRM fluorescence intensity increased in all cells, since $O_2$ is no longer reduced to $H_2O$ and protons are not pumped to the IMS (Fig. 5a and c). ATP production was partially restored after glucose addition since glycolysis was activated and compensated for OXPHOS malfunction (Fig. 5a). FRET analysis showed that both BCL2 and BCL(X)L cells maintained a higher FRET/CFP ratio compared to MCF7-pSFFV (Fig. 5b). Slope analysis for sodium azide highlighted higher values for BCL2- and BCL(X)L- overexpressing cells compared to control cell lines, suggesting a slower ATP consumption (Fig. 5d).

We performed intracellular oxygen measurement using the MitoImage™ MM2 probe (Supplementary Fig. 6B) [25, 26]. Cells treated as described in Materials and methods, were placed in KB supplemented with 2 mM pyruvate. After 30 min of baseline recording, oxygen concentration in the atmosphere was reduced to 2% (Fig. 5e). Under 2% $O_2$, cells were treated with 10 µM oligomycin and 5 mM glucose to block ATP synthase-related $O_2$ consumption. The increase in intracellular $O_2$ availability recorded was higher in the MCF7–BCL2 and BCL(X)L (Fig. 5e and f). In all, 10 µM FCCP was added to observe maximum respiration caused by permeabilization of the inner $\Delta\Psi_m$ to protons, unrelated to ATP synthase activity. Finally, $O_2$ was increased back to ambient concentration showing that 21% $O_2$ was saturating the MM2 probe again. We also employed MitoXpress®-Intra ($O_2$-sensitive cell-penetrating nanoparticle probe) to measure intracellular oxygen levels ($icO_2$) during hypoxia (1% $O_2$ concentration), together with pH (via phenol red absorbance), under the influence of different

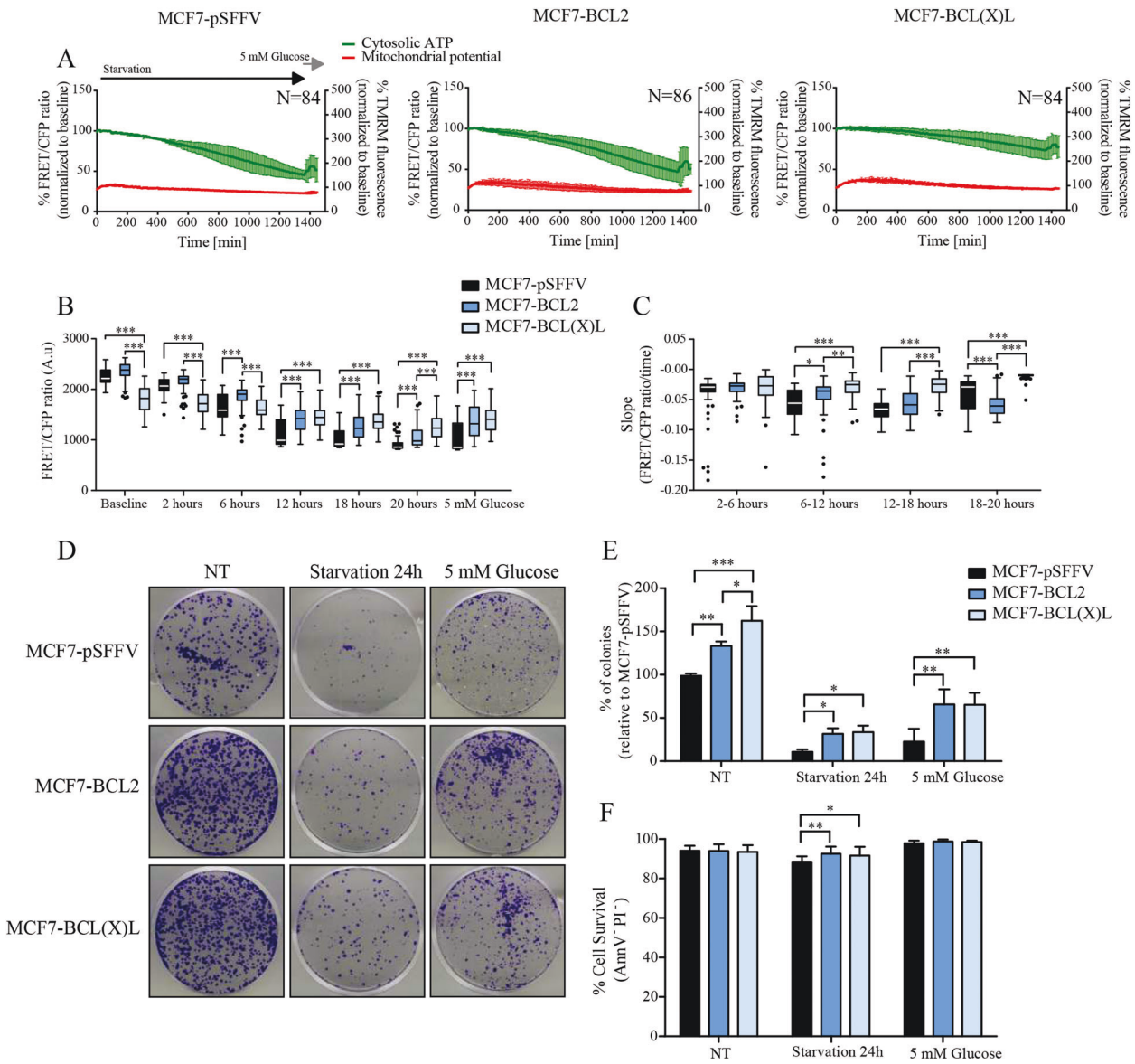


**Fig. 4 BCL2 and BCL(X)L cells maintain higher cytosolic ATP during starvation. a** Representative traces of cytosolic ATP signal and mitochondrial membrane potential. FRET/CFP ratio from ATeam probe and TMRM fluorescence were monitored simultaneously in all MCF7-ATeam clones. Cells were placed in KB with no nutrients and signals recorded every 5 min. After 23 h, 5 mM glucose was supplemented for the remaining hour. All data represent mean±SD from $n =$ 3 independent experiments and both signals are normalized to the baseline levels (each cell line normalized to its own baseline). **b** The absolute FRET/CFP ratio was analyzed by taking into account the minimal value reached by the probe at each time point selected. **c** Slope values of the decrease in cytosolic ATP, during starvation, were assessed by dividing the ΔFRET/CFP ratio to the Δtime (time offset–time onset), at the indicated time points. All values were analyzed by two-way ANOVA with Tukey post test (* indicates a $p$ value < 0.05, ** indicates a $p$ value < 0.01, *** indicates a $p$ value < 0.001). **d** Clonogenic assay of MCF7 clones in full medium (NT), starvation medium (SILAC medium plus dialyzed FBS with no glucose and no glutamine) and reduced glucose medium (SILAC medium plus dialyzed FBS with 5 mM glucose and no glutamine). In the case of starvation, the medium was replaced with full RPMI after 24 h. Clonogenic potential was assayed after 7 days in culture. **e** Colonies were counted using OpenCFU software and the change in colony growth was normalized to non-treated (NT) MCF7-pSFFV cells. **f** Percentages of surviving cells (Annexin V-/PI fraction) in non-treated (NT), starved and reduced glucose conditions. Bars represent means ± SD from three independent experiments. One-way ANOVA with Tukey post test was used to assess significance (* indicated a $p$ value < 0.05, ** indicates a $p$ value < 0.01, *** indicates a $p$ value < 0.001).

substrates. Cells were incubated in SILAC medium plus dialyzed FBS with 2 mM of glucose, pyruvate or lactate, without glutamine (see Materials and methods for details). As shown in Supplementary Fig. 7A we recorded a decrease in $icO_2$ after switching to hypoxia. $icO_2$ reached a different plateau among the clones, with BCL(X)L highlighting higher values in glucose (Supplementary Fig. 7A). We analyzed the slope of oxygen-consumption kinetics and

found that in glucose, MCF7–BCL(X)L-overexpressing MCF7 possessed slower $O_2$ consumption rates, when compared to MCF7-pSFFV and BCL2. Both BCL2 and BCL(X)L cells showed slower consumption kinetics in 2 mM lactate (Supplementary Fig. 7C), while in 2 mM pyruvate, only BCL2 cells showed slower oxygen consumption when compared to the other clones (Supplementary Fig. 7C). pH simultaneously decreased with different kinetics from 7.2 to 7.1, in 2 mM lactate or pyruvate (Supplementary Fig. 7B), while in glucose, pH reached 7.0 in all clones after 10 h of hypoxia (Supplementary Fig. 7B). We analyzed slopes for the pH decrease and found that in 2 mM glucose, MCF7–BCL2- and BCL(X)L-overexpressing cells exhibited decreased slope values compared to MCF7-pSFFV cells, highlighting a faster acidification of the medium (Supplementary Fig. 7D). On the other hand, in lactate and pyruvate, only MCF7–BCL(X)L showed higher pH slope values compared to MCF7-pSFFV and BCL2,

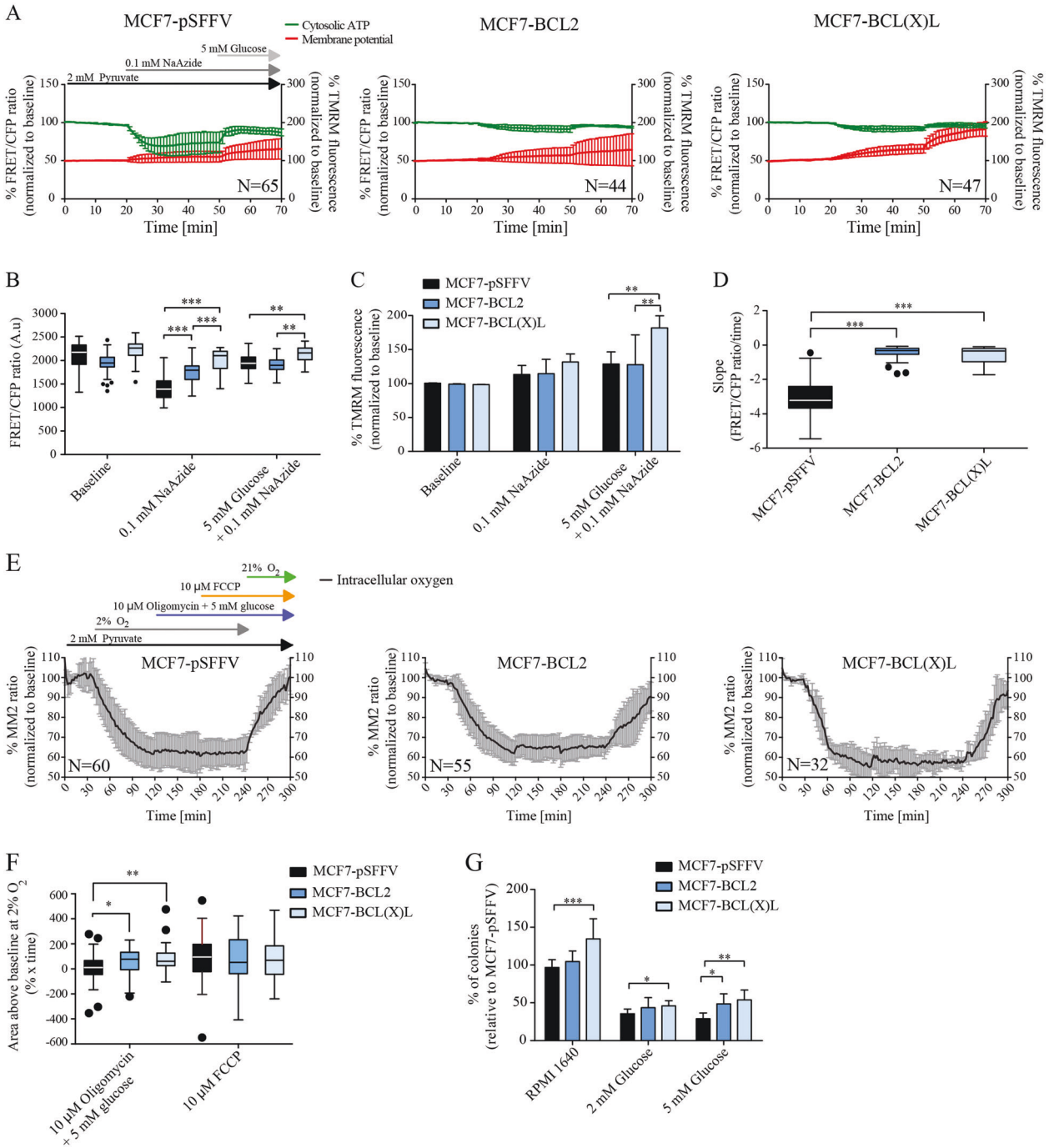

◀ **Fig. 5 BCL2 and BCL(X)L maintain higher cytosolic ATP after sodium azide treatment and regulate oxygen consumption during hypoxia. a** Representative traces of cytosolic ATP signal and mitochondrial membrane potential. FRET/CFP ratio kinetics from ATeam probe and TMRM fluorescence were monitored, in all MCF7-ATeam clones. Cells were placed in KB with pyruvate; baseline was recorded for 20 min and 0.1 mM NaAzide was added into the medium. After 30 min of treatment, 5 mM glucose was supplemented for the last 20 min. All data represent mean ± SD from $n = 3$ independent experiments and both signals are normalized to the baseline levels (each cell line normalized to its own baseline). **b** The absolute FRET/CFP ratio was analyzed by taking into account the minimal value reached by the probe after NaAzide addition and maximal value after glucose addition. **c** TMRM-intensity values normalized to the baseline levels from TMRM kinetics were analyzed by taking into account the maximal value reached after each treatment. **d** Slope values of sodium azide addition were assessed by dividing the ΔFRET/CFP ratio to the Δtime (time offset – time onset). All values were analyzed by two-way ANOVA with Tukey post test (* indicates a $p$ value < 0.05, ** indicates a $p$ value < 0.01, *** indicates a $p$ value < 0.001). **e** Kinetics of intracellular oxygen levels were measured with MitoImageTM (MM2) and normalized to baseline at 21% $O_2$. After reduction of the atmospheric $O_2$ from 21 to 2%, cells were treated with 10 µM oligomycin and 5 mM glucose followed by 10 µM FCCP, and the atmospheric $O_2$ was set back to 21% before the end of the experiment in all MCF7 clones, as indicated on top of the left graph for MCF7-pSFFV. All data represent mean ± SD from a minimum of 3 independent experiments. **f** Area above baseline (at 2% oxygen) for oligomycin + glucose and FCCP treatments. Addition of oligomycin and glucose inhibits mitochondrial ATP synthesis; with the increase in the intracellular $O_2$, the $O_2$ consumption in BCL2- and BCL(X)L-overexpressing cells was decreased, due to the activity of the ATP synthase, than in the pSFFV clone. One-way ANOVA with Tukey post test was used to assess significance (* indicated a $p$ value < 0.05, ** indicates a $p$ value < 0.01, *** indicates a $p$ value < 0.001). **g** Clonogenic assay of MCF7 clones in full RPMI medium (11 mM glucose) and SILAC medium plus dialyzed FBS and 2 mM or 5 mM glucose, respectively, in hypoxic conditions (1% oxygen). Colonies were counted using OpenCFU software and the change in colony growth was normalized to non-treated (NT) MCF7-pSFFV cells. All values were analyzed by two-way ANOVA with Tukey post test (* indicates a $p$ value < 0.05, ** indicates a $p$ value < 0.01, *** indicates a $p$ value < 0.001). Bars represent means ± SD from three independent experiments.

highlighting a slower medium acidification (Supplementary Fig. 7D). We also measured clonogenic potential of MCF7 clone growth in hypoxia and medium containing 2 mM or 5 mM glucose to simulate tumor microenvironment (Supplementary Fig. 7E). We observed that MCF7–BCL(X)L cells grew a higher number of colonies in all conditions, while MCF7–BCL2 showed a similar effect in 5 mM glucose, when compared to pSFFV cells (Fig. 5h).

## BCL2 and BCL(X)L silencing reduces mitochondrial ATP production following pyruvate addition and reduces clonogenic potential of MCF7 cells

To confirm our results, we employed siRNA to selectively silence BCL2 or BCL(X)L in MCF7-pSFFV cells. As shown in Supplementary Fig. 8A and B, BCL2 and BCL(X)L protein levels were reduced by the respective siRNAs. Subsequently, we co-transfected the cells with control (ctrl), BCL2 or BCL(X)L siRNA together with the mitoATeam FRET probe, and performed the pyruvate experiment of Fig. 2 (Supplementary Fig. 9). As shown in Fig. 6a, we observed an increase in mitochondrial ATP production. However, BCL2 or BCL(X)L-silenced cells registered decreased ATP production kinetics when compared to MCF7-pSFFV (Fig. 6a). We analyzed the absolute FRET/CFP ratio and observed that BCL(X)L siRNA-treated cells possessed lower ATP level, when compared to control siRNA. A trend was seen when comparing BCL2 to control siRNA (Fig. 6b). Of note, we found that BCL2 siRNA-treated cells accumulated lower TMRM fluorescence after oligomycin (Fig. 6c) but higher baseline absolute TMRM (Fig. 6d) when compared to control or BCL(X)L siRNA. To confirm these results, we repeated similar experiment in the MDA-231 breast cancer cell lines, since these accumulate high levels of BCL2 and BCL(X)L [27]. Both BCL2- and BCL(X)L-silenced cells recorded lower mitochondrial ATP levels following pyruvate addition, when compared to ctrl siRNA-transfected cells (Supplementary Fig. 8F). Moreover, we analyzed the clonogenic potential of cells transfected with the different siRNA and found that both BCL2 and BCL(X)L siRNA-treated cells highlighted a lower number of colonies after 7 days when compared to control siRNA (Fig. 6e and f). No cell death was recorded under the same conditions (Fig. 6g), suggesting a potential block in proliferation upon reduction of BCL2 and BCL(X)L protein levels.

## BCL2 and BCL(X)L overexpression improves cell growth and migration in low-nutrient conditions

We tested whether overexpression of BCL2 and BCL(X)L could also enhance growth and migration of breast cancer cells. MCF7 clones were placed in full RPMI or SILAC medium plus dialyzed FBS with 2 mM glucose (without glutamine), and an acid phosphatase assay used to infer the number of cells. No change in growth was recorded in MCF7 cells placed in full RPMI (Fig. 7a). However, in 2 mM glucose, we found that BCL2- and BCL(X)L-overexpressing cells showed a higher number of cells after 4–6 days when compared to MCF7-pSFFV (Fig. 7b). We then performed a wound-scratch assay to measure the changes in migration after 24, 48 and 72 h (Supplementary Fig. 10). We found that both BCL2- and BCL(X)L-overexpressing MCF7 showed a reduced wound area in RPMI, when compared to control cells (Fig. 7c). Similar results were obtained for cells in 2 mM glucose medium at 48- and 72-h time points (Fig. 7d), suggesting that BCL2- and BCL(X)L-overexpressing cell lines possess higher proliferation rates and improved migratory capacity during metabolic stress.

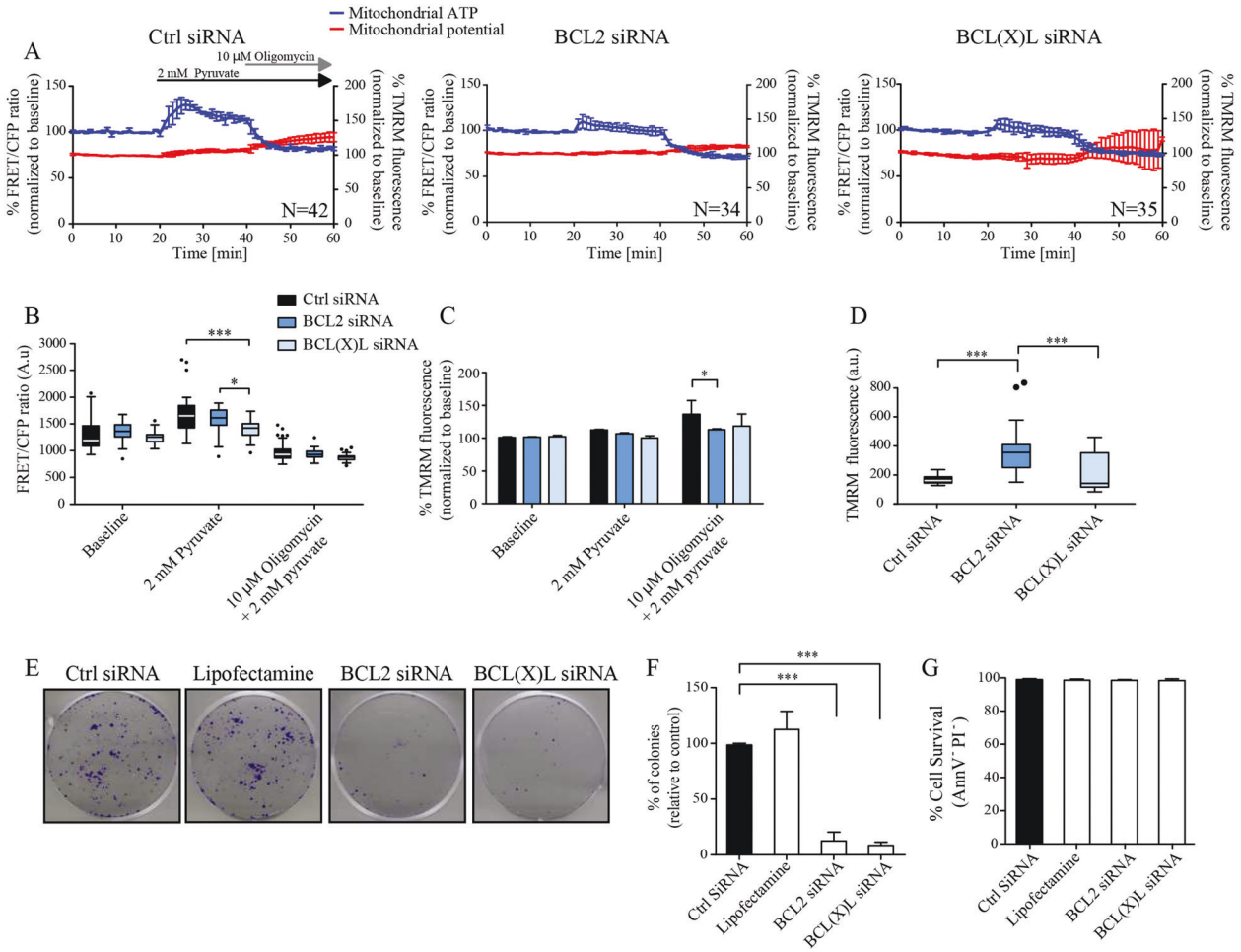


**Fig. 6 BCL2 and BCL(X)L silencing decreases ATP production following pyruvate addition and decreases clonogenic potential.** **a** Representative traces of mitochondrial ATP signal and mitochondrial membrane potential in siRNA co-transfected cells. FRET/CFP ratio kinetics from mitoATeam probe and TMRM fluorescence were monitored simultaneously in MCF7-pSFFV. Cells were starved for 3 h; after that, a baseline was recorded for 20 min and 2 mM sodium pyruvate was added into the medium. After 20 min of treatment, 10 µM of oligomycin was supplemented for the last 20 min. All data represent mean ± SD from $n = 3$ independent experiments and both signals are normalized to the baseline levels (each cell line normalized to its own baseline). **b** The absolute FRET/CFP ratio was analyzed by taking into account the maximal value reached by the probe after pyruvate addition and minimal value after oligomycin. **c** TMRM-intensity values normalized to the baseline levels from TMRM kinetics were analyzed by taking into account the maximal value reached after each treatment. **d** TMRM fluorescence absolute values obtained from baseline. All values were analyzed by two-way ANOVA with Tukey post test (* indicates a $p$ value < 0.05, ** indicates a $p$ value < 0.01, *** indicates a $p$ value < 0.001). **e** Clonogenic assay of MCF7 cells treated with control, BCL2 or BCL(X)L siRNA and Lipofectamine in full medium. Clonogenic potential was assessed after 7 days in culture. **f** Colonies were counted automatically with OpenCFU and the change in colony growth was normalized to control siRNA-treated cells. **g** Percentages of surviving cells (Annexin V-/PI fraction) in the same conditions. Bars represent means ± SD from $n = 3$ independent experiments. One-way ANOVA with Tukey post test was used to assess significance (* indicated a $p$ value < 0.05, ** indicates a $p$ value < 0.01, *** indicates a $p$ value < 0.001).

## Gene expression analysis reveals different profiles for respiratory chain complexes

Finally, in order to elucidate potential gene expression changes and mechanisms responsible for the effects of BCL2 and BCL(X)L in modulating mitochondrial bioenergetics, we performed RNA-seq experiments of the three MCF7 cell lines. Moreover, we compared these data with gene expression profiles from publicly available breast cancer cell lines and patient samples. For our in-house dataset, we found that pSFFV and BCL2 clones showed similar expression patterns. Higher expression in pSFFV- and BCL2-overexpressing cell lines compared to BCL(X)L cells has been found for the majority of respiratory chain complexes. Nonetheless, COX1, COX2 and COX3 (Complex IV) displayed the lowest and highest expression in BCL(X)L and BCL2 clones, respectively. Additionally, NDUFA11 (Complex I) expression was the lowest in the MCF7-pSFFV cells and increased in the overexpressing clones. UQCRC1 (Complex II) expression was found

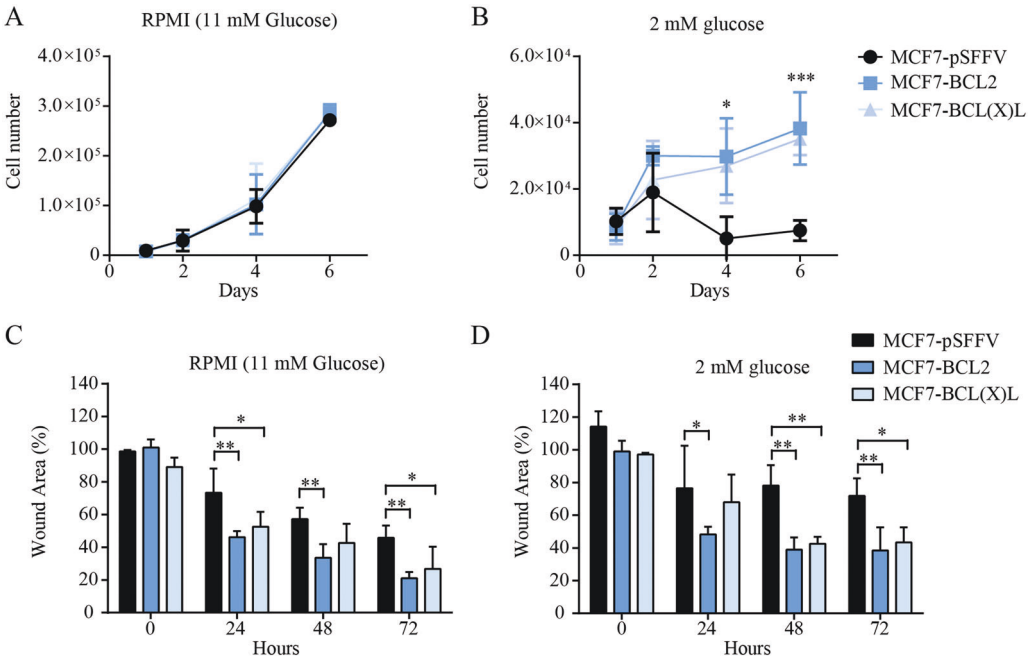


**Fig. 7 BCL2 and BCL(X)L overexpression increases proliferation and migration properties in glucose-limiting conditions. a**, **b** Cell numbers obtained from acid phosphatase assay for MCF7 clones in full RPMI (11 mM glucose) and SILAC medium plus dialyzed FBS with 2 mM glucose, respectively. **c**, **d** Wound- healing assay for MCF7 clones in full RPMI (11 mM glucose) and SILAC medium plus dialyzed FBS with 2 mM glucose, respectively. Bars represent means ± SD from $n = 3$ independent experiments. All values were analyzed by two-way ANOVA with Tukey post test (* indicates a $p$ value < 0.05, ** indicates a $p$ value < 0.01, *** indicates a $p$ value < 0.001).

altered only in the BCL(X)L-overexpressing cells (Fig. 8). We investigated the association between the expression of BCL2 and BCL(X)L (BCL2L1) with the expression of the 40 genes found to be statistically and significantly different in the analysis of the MCF7 clones in publicly available datasets derived from cell lines (CCLE, $n = 50$), patient-derived breast cancer xenografts ($n = 38$ PDXs, Supplementary Figure 11) [28] and tumor resections from the METABRIC ($n = 1904$) collection. We found that COX1, COX2 and COX3 gene expression is negatively correlated with BCL2 (small blue dots), consistent with our in-house data, showing a lower expression of these genes in the BCL2-overexpressing clones than in the pSFFV controls. Furthermore, COX1, COX2 and COX3 were found to be positively correlated with BCL(X)L gene expression, also consistent with findings in our cell lines.

## Discussion

In this work, we described the role of BCL2 and BCL(X)L in regulating breast cancer bioenergetics. Absolute concentrations of the overexpressed proteins were found to be similar to the levels seen in breast cancer patients and other cancer patients [16, 20], or breast tumor xenografts [29, 30]. We found that overexpression of either of these proteins improved ATP consumption (the ability to consume metabolites)/production (efficiency to synthesize ATP) after various metabolic or toxic challenges.

We highlighted that the addition of low pyruvate concentrations increased mitochondrial ATP synthesis, in line with other studies showing that cancer cells employ OXPHOS [31–33]. Overexpression of BCL2 or BCL(X)L did not increase mitochondrial ATP production after starvation. Interestingly, after pyruvate addition, NAD(P)H production rates were slower in BCL2 and BCL(X)L cells when compared to MCF7-pSFFV, suggesting that these cells produced similar amounts of mitochondrial ATP by consuming/producing less NAD(P)H. Moreover, BCL2- and BCL(X)L-overexpressing cells accumulated higher levels of NAD(P)H, pointing to an improved bioenergetics status of these cells. Interestingly, we found that levels of NDUFA11 (Complex I) were higher in overexpressing cell lines.

FCCP (and sodium azide) will impair mitochondrial function and elucidate if ATP is still synthesized under conditions where cells can only employ pyruvate as the source of energy, and glycolysis is not occurring. Oligomycin will specifically and directly impair ATP synthesis and highlight if ATP synthase is more efficiently working, even when $\Delta\Psi_m$ is hyper-polarized. Indeed, these treatments highlighted an increased respiratory capacity of BCL2- and BCL(X)L-overexpressing cells. In fact, FCCP and oligomycin appeared to be more 'effective' in

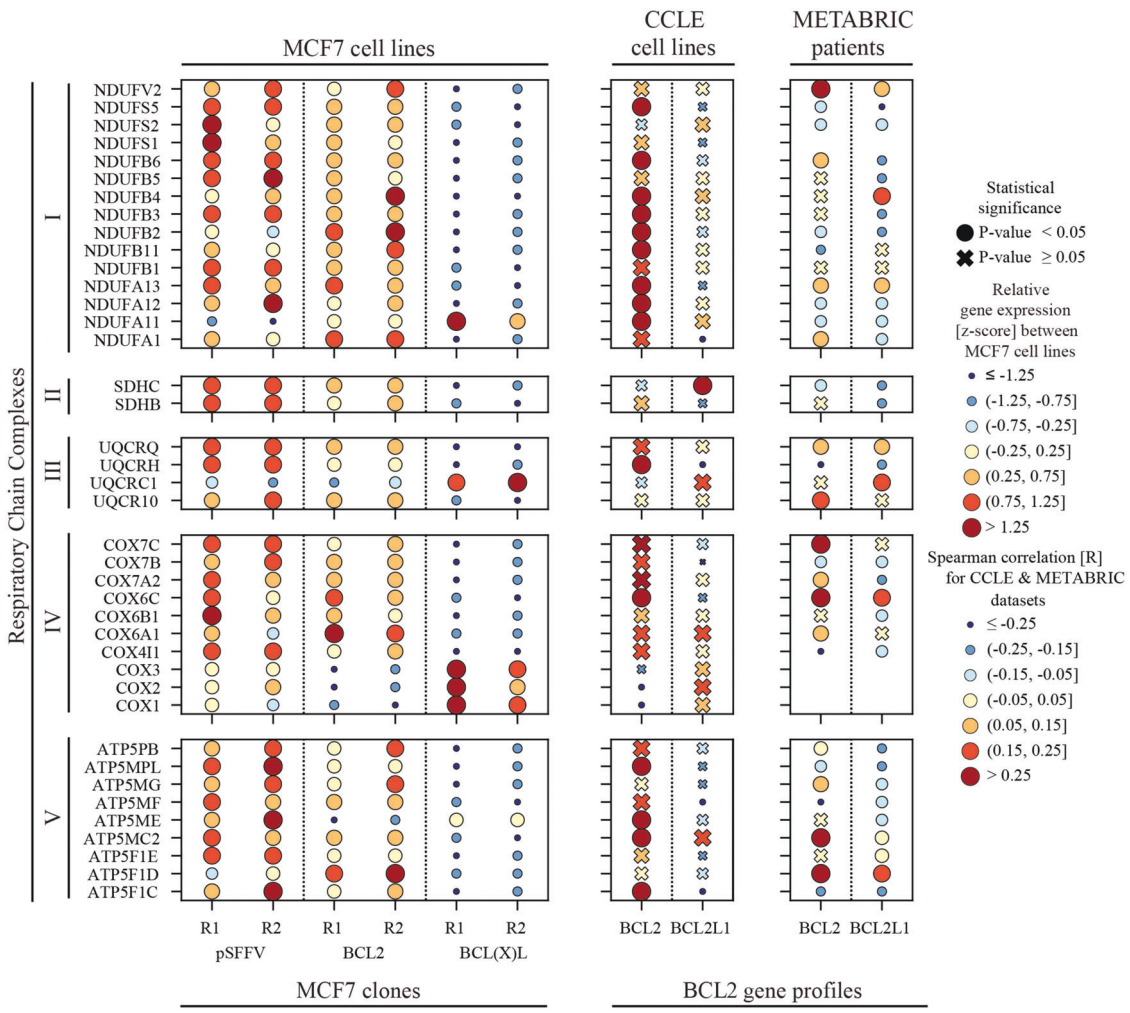


**Fig. 8 Gene expression analysis of the respiratory chain in relation to BCL2 and BCL(X)L in MCF7 clones, CCLE and METABRIC datasets.** Comparison between expression of the genes from the respiratory chain, grouped by complex. For the in-house dataset, the relative gene levels, expressed as rlog-normalized and z-scored values, for the control, BCL2- and BCL(X)L-overexpressing clones (in duplicates, R1 and R2) are size- and color-coded (lower in blue, higher in red). Only genes that were statistically significantly different (non-adjusted $p$ values < 0.05; $n = 40$ out of $n = 96$ tested genes) are included in the figure. The statistical output, including the effect size and comparison between individual cell lines for the complete set of genes that mapped to the complexes ($n = 96$), is reported in Supplementary Table 1. For the other datasets, we used the expression at the transcript level (BCL2 and BCL2L1). The association effect size expressed as Spearman correlation between BCL2 or BCL(X)L and each gene was size- and color-coded similarly to the data from the MCF7 clones to facilitate comparison. Genes with statistically significant correlation with BCL2 or BCL(X)L expression were annotated in the figure. The statistical output, including effect size and $p$ values (unadjusted) for all the tested genes, is included in Supplementary Table 2. For the CCLE, METABRIC datasets (Fig. 8) and Gao PDX (Supplementary Fig. 11) positive correlation is indicated in a bigger red dot and negative correlation with a smaller blue dot.

MCF7-pSFFV cells, when compared to cells overexpressing BCL2 and BCL(X)L, suggesting that both proteins improve coupled respiration and reduce the proton leak. We also found that BCL(X)L cells accumulated higher $\Delta\Psi_m$ after oligomycin titration. This reduced proton leak may be potentially linked to VDAC activity regulation by BCL2 proteins [34, 35], or the ability of BCL2 proteins to form ion channels in lipid bilayers [36]. In our study, we did not observe differences in levels of the ATP synthase subunit β, or in ATP synthase activity between MCF7 control and BCL2- or BCL(X)L-overexpressing cells. A previous study conducted in neurons using patch-clamp techniques, showed that BCL(X)L increased ATP synthase activity through direct binding to the β and α subunits [9]. This could suggest tissue-specific modalities of BCL2 proteins in regulating cell bioenergetics. Nonetheless, in line with our data, it has been previously shown that BCL(X)L regulates mitochondrial energetics through the stabilization of the inner $\Delta\Psi_m$ in neurons [10]. Deletion or inhibition of BCL(X)L led to large fluctuation of membrane potential by increasing futile ion flux across the inner mitochondrial membrane, enhancing the probability of an energetic crisis

during stress [10]. A different study revealed that recombinant BCL(X)L was able to restore metabolite exchange across the outer membrane, without inducing the loss of cytochrome *c* from the intermembrane space through the inhibition of VDAC closure [8]. Together, these data suggest that BCL2 proteins improve cellular bioenergetics potentially through the reduction of the proton leak or through ion exchange through the inner and outer mitochondrial membrane [8, 37].

When cells were starved, both BCL2 and BCL(X)L cells maintained higher ATP concentration and slower consumption. This was linked to higher NAD(P)H levels as such levels maintain OXPHOS for longer times [38], and high NAD(P)H autofluorescence is a marker for increased OXPHOS capacity [39]. Cardiac-specific BCL2 overexpression in mice led to increased NAD(P)H and pyruvate oxidation [40] and reduced the levels of ATP consumption post FCCP treatment [41]. The slower ATP consumption recorded in overexpressing cells likely improves their ability to grow under unfavorable conditions. Indeed, we observed increased clonogenic potential in BCL2 and BCL(X)L cells starved or grown in reduced glucose. Similar results were observed in normal conditions, suggesting that BCL2 and BCL(X)L sustained slower ATP consumption/production, therefore consuming less nutrients. This could also explain why we did not observe similar mitochondrial or cytosolic ATP levels, at baseline, across the different clones. Furthermore, BCL2 and BCL(X)L cells showed increased growth rates and migration in glucose-limiting conditions. The increased nutrient availability might sustain the surrounding cell growth increasing tumorigenic potential of BCL2- and BCL(X)L-overexpressing tumors. Moreover, stabilization of the $\Delta\Psi_m$ by BCL2 and BCL(X)L might be important for clonogenic growth of cancer cells, in addition to the observed effects on bioenergetics. Indeed, $\Delta\Psi_m$ has a role in the regulation of other processes inside the cells [42–44] and cancer cells usually accumulate higher $\Delta\Psi_m$ [45–47].

Our results also showed that both BCL2 and BCL(X)L cells maintain higher ATP levels during chemical hypoxia. Another study linked BCL2 overexpression in human leukemia cells to increased oxygen consumption and higher mitochondrial respiration rates [48]. Indeed, our intracellular oxygen imaging approach showed that when ATP synthesis was blocked, BCL2- and BCL(X)L- overexpressing cells showed decreased $O_2$ consumption, indicating a close link of $O_2$ consumption to the activity of the ATP synthase. These effects could depend on altered levels of cytochrome c oxidase found in our gene expression analysis. When oxygen concentration was decreased to 1%, under different substrate availability, BCL2 and BCL(X)L cells registered slower oxygen depletion, indicating a potential improved adaptation to hypoxia. Indeed, when cells were cultured in glucose- limiting conditions, both BCL2 and BCL(X)L cells showed a higher clonogenic potential.

In conclusion, we found that BCL2 or BCL(X)L overexpression can increase the resistance of tumor cells to metabolic stress independent of apoptosis inhibition, by more efficiently coupling the mitochondrial proton motive force with ATP production. The effects reported in this paper may be important contributors to the oncogenic activity of BCL2 family proteins and the survival of cancer cells in a metabolically stressed tumor microenvironment.

## Materials and methods

### Materials and reagents

Faetal bovine serum, tetramethylrhodamine methyl ester (TMRM) and Lipofectamine® 2000 were from Invitrogen (Bio Sciences). RPMI 1640 medium, Oligomycin, Carbonyl cyanide 4-(trifluoromethoxy)phenylhydrazone (FCCP), staurosporine, crystal violet, phenol red, sodium pyruvate, D-glucose, 2-deoxy-D-glucose, L-glutamine, L-arginine, L-lysine and 4-Nitrophenyl phosphate disodium salt hexahydrate came from Sigma-Aldrich. Cisplatin (CDDP) was purchased from Selleckchem. Glass-bottom dish (35×10) 12 mm aperture used for time-lapse imaging was from WillCo Wells BV. SILAC™ RPMI 1640 Flex Media and dialyzed faetal bovine serum were purchased from Thermo Scientific.

### Cell lines

MCF7-pSFFV, MCF7–BCL2 and MCF7–BCL(X)L were cultured in RPMI 1640 supplemented with 100 U/mL of penicillin/streptomycin, 10% faetal bovine serum and incubated at 37 °C in humidified atmosphere with 5% of $CO_2$. Where specified, MCF7 clones were placed under SILAC with dialyzed FBS, 0.2 g/L arginine, 0.04 g/L lysine and 0.0053 g/L phenol red, without glutamine and with/without the presence of glucose. Cell lines were free of mycoplasma.

### Plasmids and transfection

The ATeam1.03-nD/nA/pcDNA3 and MitoATeam1.03 probes [22] were kindly provided by Prof. Hiroyuki Noji (Osaka University) and Prof. Hiromi Imamura (Kyoto University). Cells were seeded at a density of $2*10^3$ onto prewashed, poly-D-lysine (5 µg/ml)-coated glass WillCo dishes (WillCo Wells BV) and incubated overnight at 37 °C with 5% $CO_2$. Twenty-four hours following seeding, a transfection mix was prepared that consisted of 70 µL of Opti-MEM, 0.7 µL of Lipofectamine 2000 and 0.2 µg/µL of

DNA. After 20 min of incubation at RT, the medium from each dish was removed, and the transfection mix pipetted onto the cells. Plates were then incubated for 4 h at 37 °C. Finally, the media containing this transfection mix was removed and 2 mL of fresh medium added to each dish.

## Generation of cytosolic ATeam stable clones

MCF7-pSFFV, MCF7–BCL2 and MCF7–BCL(X)L were seeded in 6-well plates at a density of $1*10^6$ cells per well. Cells were transfected with 200 ng of ATeam plasmid using Lipofectamine for 4 h in Opti-MEM medium. After 24 h, transfection efficiency was assessed on a fluorescent microscope and cells cultivated to reach confluency. Subsequently, cells were tripsinized, diluted 1 in 100 and seeded in new 6-well plates. After 7 days, cells were observed for the presence of fluorescent colonies. Positive cells carrying ATeam plasmid were then picked up with a p200 pipette, placed in 2 ml of medium, gently separated and moved to a new 6-well plate. The same procedure was then repeated 2–3 times to insure 90–100% of positive-fluorescent colonies. Cells were then left to reach confluency and moved to a 25 flask and grew regularly.

## Western blotting and BCL2 profiling

Cells were scraped, collected and lysed in RIPA buffer (150 mM NaCl, 1.0% IGEPAL® CA-630, 0.5% sodium deoxycholate, 0.1% SDS, 50 mM Tris, pH 8.0, protease and phosphatase inhibitors mix 1:100). Protein concentration was determined with micro BCA (bicinchoninic acid) assay (Pierce, Rockford, IL) and a total of 30 µg of protein loaded into a SDS gel after complete denaturation at 90 °C for 10 min in Laemmli buffer. The samples were then transferred to nitrocellulose membrane and blocked in TBS-T/5% milk for 1 h. Primary antibodies to MCL1 (1:250, BD Biosciences), BCL2 (1:100, Santa Cruz Biotechnology), BCL (X)L (1:250, Santa Cruz Biotechnology, Inc.), ATP synthase sub. β (1:1000, Invitrogen) and tubulin (1:5,000, Sigma) were mouse monoclonal. Antibodies to BAK (1:250, Santa Cruz Biotechnology, Inc.) and BAX (1:1,000, Upstate Biotechnology) were rabbit polyclonal. The horseradish peroxidase (HRP)-conjugated secondary antibodies were from Jackson ImmunoResearch (1:5000). Detection of protein bands was carried out using chemiluminescence (EMD Millipore) on a LAS-3000 Imager (FUJIFILM UK Ltd). BCL2 profiling and absolute protein concentration was carried on as previously described [20] and all densitometry analysis was performed with ImageJ. Briefly, standard calibration curves were constructed with varying concentrations (0.1–10.0 ng) of recombinant BCL2 proteins and HeLa extract, by plotting blot intensity against mass of loading. Cellular concentrations for BCL2 proteins in cellular lysates were calculated from calibration curves, considering HeLa cell volume of 3.1 pL [20] and the appropriate molecular weights for BAK, BAX, BCL2, BCL (X)L and MCL1.

## Immunofluorescence of BCL2 and BCL(X)L

MCF7 cell lines were cultured on 13 mm coverslips for 24 h. On the next day, cells were stained for 30 min at 37 °C with MitoTracker Red CMXRos (Thermo Fisher Scientific) to stain mitochondria, subsequently fixed with 4% paraformaldehyde (PFA, Affymetrix) for 10 min and permeabilized with 95% ethanol and 5% glacial acetic acid. For detection of BCL2, a mouse monoclonal anti-BCL2 (clone 8E12, Thermo Fisher Scientific) and an Alexa Fluor® 488-conjugated secondary anti-mouse (Thermo Fisher Scientific) were used. For immunostaining of BCL(X)L, a rabbit monoclonal anti-BCL(X)L (clone 54H6, Cell Signaling) and an Alexa Fluor® 488-conjugated secondary anti-rabbit (Thermo Fisher Scientific) were used. Coverslips were mounted on a microscope slide with ProLong® Gold Antifade Mountant (Thermo Fisher Scientific) with DAPI to visualize nuclei. Imaging was performed with a LSM 710 confocal microscope (Carl Zeiss, Germany) using 405, 488 and 561 nm for DAPI, Alexa Fluor 488 and MitoTracker Red laser excitation, respectively, and using the proper emission bands of the detection unit. Each field of view was acquired with a stack covering the whole-cell body with an optical slice thickness of 1 µm (FWHM) and steps of 0.20 mm with a 100 × 1.4 NA oil-immersion plan apochromat objective. Subsequently, the stacks were de-convolved using Autoquant X (version 2.1.0, Media Cybernetics, UK) and images further processed with ImageJ 1.45 s (National Institutes of Health, Bethesda, MD, USA).

## Flow cytometry

Cells were treated with 40 µM cisplatin and 2 µM STS for 24 h at 37 °C. After incubation time, cells were collected by tripsinization and stained with Annexin V-FITC and propidium iodide (Biovision) for 20 min at room temperature in dark conditions and analyzed using a CyFlow ML (Partec) flow cytometer and FloMax software. A minimum of 10,000 events were recorded for each sample. Surviving cells were defined as the fraction of Annexin V- and PI-negative cells. The percentage of apoptotic cells was defined as Annexin V positive/PI negative plus Annexin V positive/ PI positive.

## Clonogenic assay

MCF7 cell lines were seeded at a density of 1000 cells per well in a six-well plate. Starvation conditions were

mimicked by using SILAC medium (Thermo Scientific) with dialyzed FBS (Thermo Scientific), 0.2 g/L arginine, 0.04 g/L lysine and 0.0053 g/L phenol red (Sigma-Aldrich). No glucose or glutamine was added to the medium. After 24 h of treatment, the cell medium was replaced with fresh RPMI 1640. In all, 5 mM glucose medium was achieved by using the above- described SILAC medium with the addition of 5 mM D-glucose. After a week of incubation, cells were washed and fixed with 4% PFA (Affymetrix) and stained with 0.5% crystal violet. Plates were scanned on a CanoScan LiDE 80 (Canon) at a resolution of 1200 ppi. Images were then cropped with ImageJ and analyzed with OpenCFU software [49].

## Time-lapse imaging

Cells were seeded at a concentration of $2 \times 10^3$ in sterile Willco dishes and let to adhere overnight. Then, ATeam constructs were transfected according to the protocol described above. On the day of the experiment, adherent cells were washed twice with krebs-hepes buffer (KB, 140 mM NaCl, 5.9 mM KCl, 1.2 mM $MgCl_2$ and 15 mM HEPES) and the medium replaced with 1 mL of KB containing 30 nM TMRM, 2 mM sodium pyruvate and 2.5 mM $CaCl_2$; an equilibration time of 40 min was applied before starting the imaging procedure. For experiments in Fig. 2, KB with $CaCl_2$ without pyruvate was first used for 3 h, followed by replacement to KB with TMRM, $CaCl_2$ and 2 mM pyruvate. Mineral oil was added on top of the KB to prevent evaporation and the dishes transferred to a heated stage (37 °C) in a 5% $CO_2$ environment above a 63×/1.4 NA Plan-Apochromat oil-immersion objective lens on an inverted confocal laser-scanning microscope (LSM 710, Carl Zeiss). Mitochondrial ATP kinetics measurements were carried out using lasers of 405, 488 and 561 nm for excitation of FRET/CFP, YFP and TMRM, respectively, with a pixel dwell time of 2.55 µs and images taken every minute. Detection ranges were set to 445–513 nm and 513–562 nm for CFP and FRET/YFP, while 562–710 nm was used for TMRM with pinholes set to 2-µm optical sectioning (FWHM). For NAD(P)H kinetics measurement, MCF7 clones were prepared as before and the medium replaced with 1 mL of KB with 2 mM pyruvate and 2.5 mM $CaCl_2$. Mineral oil was added on top of KB to prevent evaporation and the dishes transferred to a heated stage (37 °C) in a 5% $CO_2$ environment above a 40×/1.3 Numerical Aperture (NA) Plan-Neofluar of an inverted epifluorescence microscope (Axiovert 200 M, Carl Zeiss). NAD(P)H was measured through autofluorescence as the reduced form of these molecules is different from the oxidized form as they absorb and emit light at 340 nm and 445 nm, respectively. These experiments were carried out using 25% of a HBO 100 mercury short-arc lamp for excitation with illumination wavelength of 340/20 nm for NAD(P)H excitation with an exposure time of 100 ms, and a binning of $4 \times 4$. Emission was collected at 447/60 nm and images taken every minute. All kinetics were measured for 20 min without treatment in order to obtain a baseline signal. Images were processed using ImageJ2 (National Institutes of Health, Bethesda, MD, USA) and Metamorph 7.5 (Universal Imaging Co., Westchester, PA, USA). Time-lapse sequences were imported into ImageJ and background was first subtracted from each image. After creating combined images of the three fields of views for each channel sequence, a median filter with a radius of one pixel was applied. The combined images were then processed using Metamorph. Mitochondria within cells were segmented from background using the YFP time-lapse images. The segmented mitochondrial areas were converted into a mask used to remove background values from any further analysis of the FRET/CFP stack. To this end, the FRET image stack was first multiplied by the YFP mask and divided by CFP image stack, and regions of interest were then selected for analysis.

For cytosolic ATP measurement, stable-expressing ATeam MCF7 clones were seeded in sterile Willco dishes. For the FCCP and sodium azide treatment, on the day of the experiment, KB with 30 nM TMRM, 2 mM sodium pyruvate and 2.5 mM $CaCl_2$ was added on top of the cells, with mineral oil to prevent evaporation; an equilibration time of 40 min was applied before starting the imaging procedure. For the starvation experiment, KB with 30 nM TMRM and 2.5 mM $CaCl_2$ was used instead. The dishes were transferred to a heated stage (37 °C) in a 5% $CO_2$ environment above a 40×/1.3 Numerical Aperture (NA) Plan-Neofluar oil-immersion objective lens on an inverted epifluorescence microscope (Axiovert 200 M, Carl Zeiss), used with a selected polychroic mirror and filter wheel settings. Experiments were carried out using 0.09% of a HBO 100 mercury short-arc lamp for excitation with a band pass of 438/24 nm (center wavelength and bandwidth) for FRET/CFP (cyan fluorescent protein) and a band-pass filter with 500-/24 nm YFP (yellow fluorescent protein) with exposure time of 20 ms. CFP emission was measured in the range of 483/32 nm and FRET/YFP emission in the range of 542/27 nm. TMRM was exposed to 531/40 nm for 10 ms and detected in the emission range of 593/40 nm (all filters from Semrock). For all experiments, a custom-made Metamorph journal was used to obtain the average-intensity signal from all regions, and an excel macro was then applied to sort the values and to convert them to percentage normalized to the baseline (each cell line was normalized to its own baseline). All experiments were performed at least three times independently of each other. For mitoATeam and cytosolic ATeam experiments, slope values were assessed from normalized traces: ΔFRET was calculated by subtracting the minimal fluorescence value obtained following treatment (offset) to the fluorescence value at the

onset. Δtime was calculated accordingly by subtracting the time when the probe reached the minimal value to the time at the onset. The slope over time was finally obtained by dividing ΔFRET to Δtime. For NADH experiment, a non-linear fit function (Y = Autofluorescence max*X/(Km+X)) in GraphPhad Prism was employed to obtain Km values.

## Mitochondrial isolation and ATP synthase activity assay

ATP synthase activity measurement was carried on with a commercially available kit from Abcam, following mitochondrial isolation. Mitochondria were isolated accordingly to Frezza et al. [50]. Briefly, MCF7 clones were seeded in t175 flasks and allowed to reach 80–90% confluency. Then, cells were detached, collected with fresh medium in 50-mL Falcon tubes and centrifuged at 600 × *g* for 10 min at 4 °C. The supernatant was discarded and 3 mL of ice-cold isolation buffer (0.1 M Tris–MOPS, 0.1 M EGTA/Tris, 1 M sucrose and pH at 7.4) was added. Cells were homogenized using a tissue homogenizer at 708 × *g* per 6 times, and centrifuged again at 600 × *g* for 10 min at 4 °C. Then, the supernatant was collected in a 15-mL Falcon tube and centrifuged at 7000 g for 10 min at 4 °C. The supernatant was discarded and the pellet washed with 200 µL of ice-cold isolation buffer, resuspended in 200 µL and transferred to a 1.5-mL Eppendorf tube. The homogenate was then centrifuged at 7,000 g for 10 min at 4 °C, supernatant discarded and the pellet resuspended in 50 µL of ice-cold isolation buffer. The homogenate sample underwent 2 cycles of freeze–thaw, and then centrifuged at 16,100 × *g* for 10 min at 4 °C. The sample was then diluted with 100 µL of solution 1 from the kit, and the protein concentration assessed with BCA assay. Protein concentration was adjusted to 5.5 mg/ml and 1/10 volume of detergent solution added. After 30 min of incubation on ice, the samples were centrifuged at 16,100 × *g* for 20 min at 4 °C and the pellet discarded. The microplate from the kit was then loaded with 50 µL of solution 1, and 2.5 µg of each sample. Empty wells with solution 1 alone were added as background control. The microplate was then stored at 4 °C overnight to let the ATP synthase enzymes bound the antibody-coated surface of each well. The next day, wells were emptied and washed with 300 µL of solution 1. Subsequently, 40 µL of lipid mix was added to each well and the microplate incubated at RT for 45 min. After incubation time, 200 µL of reagent mix was pipetted into each well and the plate inserted into the Clariostar reader at 30 °C. Absorbance was recorded at 340 nm, with a kinetic programme every minute for 2 h. An excel template was used to calculate the activity (after background subtraction and according to the manufacturer's protocol), and normalized to ATP synthase sub. β levels from western blotting (WB) experiments.

## Intracellular $O_2$ and pH measurement using MitoXpress®-Intra

Intracellular oxygen assay was performed using commercially available MitoXpress®-Intra ($NanO_2$) from Luxcel Biosciences (Cork, Ireland). This fluorophore is an $O_2$-sensitive cell-penetrating nanoparticle probe, whose phosphorence is quenched by oxygen such that the measured signal is proportional to intracellular oxygen concentration. MCF7 clones were seeded at a concentration of $1.5*10^3$ in a Nunc Micro Well 96-well optical bottom plate. After overnight incubation, the medium was removed and cells were stained with 100 µL of fresh medium containing 5 µg/mL of MitoXpress®-Intra and 1 µg/mL Hoechst 33588 for 24 h. Before the measurements, the staining medium was replaced with SILAC medium with dialyzed FBS, 0.2 g/L arginine, 0.04 g/L lysine, 0.0053 g/L phenol red and 2 mM glucose, pyruvate or lactate as indicated (without glutamine). The plate was placed in a plate reader at 37 °C, 5% $CO_2$ and 21% $O_2$ (ClarioStar, BMG Labtech, Germany). After 3 h in normoxia (21% $O_2$), oxygen was decreased to 1% through the plate reader atmospheric regulator and time-resolved fluorescence measured every 5 min for 24 h. A custom-made scripting function for the assay was employed. Fluorescent intensities were measured at delay times of 30 µs and 70 µs, with a 30 µs window time, through the bottom optic. The probe was excited at 340–400 nm and excitation was collected at 635–655 nm, using a band-pass filter. A gain of 3000 was used for all experiments. To account for changes in proliferation rates, nuclei were stained with Hoechst and the nanoprobe fluorescence values were normalized to absolute Hoechst fluorescence. We only considered data from the start of the experiment until 600 min, as no significant change was observed after 10 h, and to exclude excessive cell death due to limited nutrient and oxygen availability. Hoechst was excited at 355/20 nm and emission collected at 455/30 nm with a gain at 1500. Values were analyzed with a custom excel template to obtain intracellular oxygen concentration ($IcO_2$) based on the calibration in Fercher et al. [51] after subtraction of blank (medium without cells). Then, both $IcO_2$ and pH signals were divided by the Hoechst signal in order to account for proliferation. pH was recorded in parallel through the measurement of phenol red absorbance spectra. The wavelength range was 350–650 nm with a step width of 5 nm and a bidirectional mode was employed for the reading. An excel template was utilized to calculate the 560/440 nm ratio and the formula $\log\left[\frac{\frac{560nm}{460nm}}{0.0002}\right]/1.18$ was employed to obtain pH values. $icO_2$ slopes were measured using a one-phase exponential decay function in GraphPad Prism, while pH slopes,

obtained from measurement of phenol red absorbance spectra, were measured using a linear regression Line function in the same software.

## Monitoring changes in $O_2$ concentration using the ratiometric MM2 probe

MCF7-pSFFV, MCF7–BCL2 or MCF7–BCL(X)L cells were grown in 4-chamber glass-bottom dishes (CellView, Greiner, Germany). The nanoparticle-based phosphorescent probe, MitoImage$^{TM}$-MM2, which consists of the $O_2$-sensitive phosphorescent reporter dye (PtTFPP), $O_2$-insensitive component (PFO) embedded in a cationic polymer, was purchased from (Luxcel now Agilent, Ireland) [26, 52]. Cells were loaded with 10 µg/ml of MM2 in RPMI medium supplemented with 1% FBS medium for 16 h at 37 °C. MM2 probe-intensity ratio was recorded on an LSM 7live Duoscan confocal microscope (Carl Zeiss, Germany) equipped with a 40×, 1.3 NA Plan-Neofluar oil-immersion objective and a thermostatically regulated chamber at 37 °C in a humidified atmosphere of 5% $CO_2$ and the $O_2$ concentration as given in the figures (Pecon, Germany). The MM2 probe was excited using 5% of the 30-mW 405-nm DPSS laser, and the emission was collected through a 415–480-nm band-pass and a 570-nm long-pass filter using a 565-nm secondary dichroic to split the emission between the 2 detectors. Cells were placed in KB with the addition of 2 mM pyruvate. After baseline measurement, oxygen concentration was reduced to 2%; after 90 min, 10 µM oligomycin and 5 mM glucose were added to stop ATP synthase- related $O_2$ consumption. The signal was measured for 60 min and 10 µM FCCP added for maximum respiration for 1 h; for the last hour of the experiment, $O_2$ was increased to ambient concentration. All images were processed using ImageJ (version 1.52r, Wayne Rasband, NIH, USA). The intensity-ratio images between the PFO and the PtTFPP (FPFO/FPtTFPP) were calculated for all areas of the image with PFO and PtTFPP fluorescence above background noise and after background subtraction multiplied by 1000 to display on a 16 bit scale [25]. Measurements were then normalized to the baseline and processed in excel (Version 2016, Microscoft, USA) and Prism (version 5, GraphPad, USA).

## Acid phosphatase assay

Acid phosphatase assay was used to measure cell number based on the conversion of pNPP to p-nitrophenol by cytosolic acid phosphatase [53]. MCF7 clones were grown in a 24 well plate at a density of $3 \times 10^4$ cells per well in either RPMI 1640 or SILAC medium (with dialyzed FBS, 0.2 g/L arginine, 0.04 g/L lysine and 0.0053 g/L phenol red) with 2 mM glucose and no glutamine. After each time point (1, 2, 4 and 6 days), the medium was removed and each well was washed once with 200 µL of 1 × PBS. To each well, 100 µL of assay buffer (0.1 M sodium acetate at pH 5.0, 0.1% Triton X-100 and 7.25 mM p-nitrophenyl phosphate) was added. The plates were then incubated at 37 °C for 2 h. The reaction was finally stopped with the addition of 50 µL and color development was assayed at 405 nm using a Multiskan® EX plate reader. The non-enzymatic hydrolysis of the pNPP substrate was also determined by including wells with the assay buffer and without any cells. A standard curve, performed with the same assay, and a fixed number of cells (1000, 5000, 10,000, 50,000, 100,000 and 500,000) was used to obtain the cell number from the different wells, using excel.

## BCL2 silencing

For BCL2 protein-silencing experiments, 100 ng of siRNA-targeting BCL2 (Santa Cruz Biotechnology, sc-61899) or BCL(X)L (Santa Cruz Biotechnology, sc-43630) was transfected employing Lipofectamine. MCF7-pSFFV and MDA-231 cells were seeded at a density of $2*10^5$ in six-well plates to assess silencing efficiency by WB. After 24 h of incubation at 37 °C, cells were transfected as previously discussed. A siRNA consisting of a scrambled sequence was used as a negative control (ctrl, Santa Cruz Biotechnology, sc-7007). One day following transfection, protein lysates were prepared from each well and stored at –80 °C for further analysis. To assess the effect of BCL2 or BCL(X)L silencing on ATP production kinetics, cells were seeded on a glass wilco at a density of $2\times10^3$ cells per dish, and allowed to adhere for 24 h. Cells were then co-transfected with 100 ng of MitoAteam plasmid and 100 ng of BCL2, BCL(X)L or control siRNA, as previously described. After 24 h (48 h for MDA-231), cells were prepared for time-lapse live- cell imaging. To assess clonogenic ability and viability after BCL2 or BCL(X)L silencing, MCF7-pSFFV cells were seeded in a 6-well plate at a density of thousand cells per well and at a density of $6 \times 10^4$ in a 24-well plate for Annexin V/PI staining. Cells were incubated for 24 h and transfected with 100 ng of BCL2, BCL(X)L or control siRNA; in both cases, wells treated with Lipofectamine 2000 and no DNA was added to exclude any effect that transfection reagents might have on cell viability. Following 24 h of incubation, 2 mL of fresh medium was added to each 6-well plate and cells were allowed to grow into colonies for 7 days, while 24-well plates were to detect apoptosis rates with flow cytometry.

## Wound-healing assay

Cells were seeded at a concentration of $3 \times 10^4$ in sterile 24-well plates and let to adhere overnight. A 2-well insert from Ibidi was placed into each well, before seeding the cells. The following day, the insert was carefully removed in order to have a clear separation to follow. All clones were imaged at

selected time points (0, 24, 48 and 72 h) on a Nikon TE2000 microscope. Images were imported in ImageJ2; a Find Edges function followed by Sharpen was used to increase the contrast of the cell area compared to the wound. The LUT (lookup table) was inverted and the analyze particle function was used (size between 100,000 and 50,000,000, circularity: 0.00–1.00) with outlines shown to obtain the area of the wound. Data were then processed with excel.

## RNA-seq experiments and gene expression analysis of publicly available datasets

MCF7 clones were seeded in t25 flasks and let to adhere overnight. On the following day, cells were trypsinized, collected in Eppendorf tubes and centrifuged. RNA was extracted with TRIzol reagent (Thermo Fisher Scientific) and samples mechanically disrupted using a homogenizer. Subsequently, chloroform was added to separate an upper aqueous phase (containing RNA) from the rest. This was mixed with isopropanol and centrifuged at 12,000 × *g* at 4 °C; the resulting pellet was put in 75% ethanol and centrifuged again at 7500 × *g* at 4 °C. The pellet was let to air- dry and resuspended in RNase-free water for further quantification with Nanodrop 2000. Next, whole-transcript RNA-seq was performed on the samples. Specifically, poly-A-containing mRNA was purified from the RNA samples and RNA sequencing libraries were created using the KAPA- stranded mRNAseq Kit (Illumina), according to the manufacturer's instructions. Briefly, sequencing libraries were prepared by converting the RNA to cDNA followed by adapter ligation and enrichment of exon-coding sequences by PCR using sequence-specific probes. The resulted cDNA libraries were sequenced on a HiSeq 4000 using a flow cell generating 1 × 50 bp reads. Transcriptome profiles were created using an existing in-house bioinformatic pipeline. More specifically, after removing the optical duplicates with Clumpify and removing sequencing adapters, the reads were mapped to the human reference genome using TopHat-Bowtie and HTSeq-count was used to create gene-count matrices. Raw counts from RNA-seq experiments were normalized using DESeq2 (R library, version 1.26.0) [54] using 'rlog' as method and '~ cell_line' as design formula. ENSEMBL ids were mapped to symbols with mygene (python package, version 3.1.0). Genes involved in the respiratory chain complexes I–V (Table 1) were retrieved from the "gene names" database curated by the HGNC—HUGO Gene Nomenclature Committee (https://www.genenames.org/data/genegroup/#!/group/639). Of the 97 genes of interest, 96 were present in the dataset.

Transcriptomic data from the Cancer Cell Line Encyclopedia (CCLE) were downloaded on 2019-06-29 from the CCLE website [55]. In downstream analyses, we focused on breast cancer cell lines (set to "BRCA", $n = 50$) and on genes ($n = 40$) from the respiratory chain complexes found to be altered in the MCF7 clones. Transcriptomic data (RNASeq, FPKM) from patient-derived xenografts (PDXs) were downloaded from the supplementary materials of Gao et al. [28]. We restricted the analysis to untreated PDXs from breast cancer patients ($n = 38$) and on genes from the respiratory chain complexes found to be altered in the MCF7 clones ($n = 37$ out of 40 were found with COX1, COX2 and COX3 missing). Transcriptomic data (mRNA z-Scores, Illumina Human v3 microarray) for $n = 1904$ primary tumor samples from breast cancer patients from the "Molecular Taxonomy of Breast Cancer International Consortium" (METABRIC) [56] study were downloaded on 2020-08-07 from the cPiortal website (https://www.cbioportal.org/study/summary?id=brca_metabric). Downstream analyses included genes from the respiratory chain complexes found to be altered in the MCF7 clones ($n = 36$ out of 40 were found with NDUFS1, COX1, COX2 and COX3 missing).

**Table 1** Breakdown of genes included for each respiratory chain complex.

| Complex | # genes |
|---|---|
| Complex I | 44 |
| Complex II | 4 |
| Complex III | 10 |
| Complex IV | 19 |
| Complex V | 20 |

We investigated the dependency of the respiratory chain complexes by BCL2 family members by comparing the expression of the mitochondrial genes listed above in parental (pSFFV) and BCL2- or BCL(X)L-overexpressing MCF7 clones. We fitted univariate regression models and evaluated statistical significance with overall ANOVA *p* values. We did not adjust *p* values for multiple comparisons as these analyses were considered exploratory. We reported pairwise cell line comparisons by TukeyHSD Post-Hoc tests and mean expression difference, 95% confidence intervals (CI, lower and upper) and *p* values (Supplementary Table 1). Next, we examined the association between BCL2 genes (BCL2 or BCL2L1) and those mitochondrial genes found to be differentially expressed in the MCF7 clones to examine whether these findings are generalizable to other cell lines, PDX models and patient tumor samples. We reported Spearman correlation as m effect-size metric and the corresponding *p* values in Supplementary Table 2.

## Statistical analysis

Data are given as means±S.D. (standard deviation). The number of independent experiments performed is indicated in the figure legends (from 3 to 5). The variance was assumed to be similar between the compared groups with a

normal distribution. For statistical comparison, two-way analysis of variance (ANOVA) or one-way analysis followed by Tukey's post hoc test was employed. $p$ values < 0.05 were considered to be statistically significant.

## Data availability

The raw and processed RNA sequencing data for the MCF7 cell lines generated in this study are publicly available in GEO (reference number GSE158808).

## Code availability

Processing and analysis code for the transcriptomic-based analysis is publicly available and archived at Zenodo (https://doi.org/10.5281/zenodo.4058036).

**Acknowledgements** We thank Dr Claus Reimertz for generating the BCL2- and BCL(X)L-overexpressing clones, and Dr Bram Boeckx for RNA sequencing. This research was funded by grants from the Irish Cancer Society Collaborative Cancer Research Centre BREAST-PREDICT (CCRC13GAL) and Science Foundation Ireland and the Health Research Board (13/IA/1881, 16/US/3301) to JHMP. We kindly thank Prof Hiroyuki Noji (Osaka University) and Prof. Hiromi Imamura (Kyoto University) for providing the mitoATeam and cytosolic ATeam plasmids. We also thank Luise Halang and Aisling O'Brien for technical assistance.

**Author contributions** Conception and design: FL, HD, and JHMP; Acquisition of data: FL, HD, MS, AUL, and DL; Writing, review and/or revision of the paper: FL, MS, HD, and JHMP; Study supervision: JHMP

## Compliance with ethical standards

**Conflict of interest** The authors declare that they have no conflict of interest.

**Publisher's note** Springer Nature remains neutral with regard to jurisdictional claims in published maps and institutional affiliations.

## References

1. Czabotar PE, Lessene G, Strasser A, Adams JM. Control of apoptosis by the BCL-2 protein family: implications for physiology and therapy. Nat Rev Mol Cell Biol. 2014;15:49–63.
2. Aouacheria A, Baghdiguian S, Lamb HM, Huska JD, Pineda FJ, Hardwick JM. Connecting mitochondrial dynamics and life-or-death events via Bcl-2 family proteins. Neurochem Int. 2017;109:141–61.
3. Autret A, Martin SJ. Emerging role for members of the Bcl-2 family in mitochondrial morphogenesis. Mol Cell. 2009;36:355–63.
4. Gross A, Katz SG. Non-apoptotic functions of BCL-2 family proteins. Cell Death Differ. 2017;24:1348–58.
5. Rolland SG, Conradt B. New role of the BCL2 family of proteins in the regulation of mitochondrial dynamics. Curr Opin Cell Biol. 2010;22:852–8.
6. Westermann B. Bioenergetic role of mitochondrial fusion and fission. Biochim Biophys Acta. 2012;1817:1833–8.
7. Brenner C, Cadiou H, Vieira HL, Zamzami N, Marzo I, Xie Z, et al. Bcl-2 and Bax regulate the channel activity of the mitochondrial adenine nucleotide translocator. Oncogene. 2000;19:329–36.
8. Vander Heiden MG, Li XX, Gottleib E, Hill RB, Thompson CB, Colombini M. Bcl-xL promotes the open configuration of the voltage-dependent anion channel and metabolite passage through the outer mitochondrial membrane. J Biol Chem. 2001;276:19414–9.
9. Alavian KN, Li H, Collis L, Bonanni L, Zeng L, Sacchetti S, et al. Bcl-xL regulates metabolic efficiency of neurons through interaction with the mitochondrial F1FO ATP synthase. Nat Cell Biol. 2011;13:1224–33.
10. Chen YB, Aon MA, Hsu YT, Soane L, Teng X, McCaffery JM, et al. Bcl-xL regulates mitochondrial energetics by stabilizing the inner membrane potential. J Cell Biol. 2011;195:263–76.
11. Perciavalle RM, Stewart DP, Koss B, Lynch J, Milasta S, Bathina M, et al. Anti-Apoptotic MCL-1 Localizes to the Mitochondrial Matrix and Couples Mitochondrial Fusion to Respiration. Nat Cell Biol. 2012;14:575–83.
12. Boroughs LK, DeBerardinis RJ. Metabolic pathways promoting cancer cell survival and growth. Nat Cell Biol. 2015;17:351–9.
13. Mason EF, Rathmell JC. Cell metabolism: an essential link between cell growth and apoptosis. Biochimica et biophysica acta. 2011;1813:645–54.
14. Dawson SJ, Makretsov N, Blows FM, Driver KE, Provenzano E, Le Quesne J, et al. BCL2 in breast cancer: a favourable prognostic marker across molecular subtypes and independent of adjuvant therapy received. Br J Cancer. 2010;103:668–75.
15. Keitel U, Scheel A, Thomale J, Halpape R, Kaulfuss S, Scheel C, et al. Bcl-xL mediates therapeutic resistance of a mesenchymal breast cancer cell subpopulation. Oncotarget. 2014;5:11778–91.
16. Lindner AU, Lucantoni F, Varešlija D, Resler A, Murphy BM, Gallagher WM, et al. Low cleaved caspase-7 levels indicate unfavourable outcome across all breast cancers. J Mol Med (Berl). 2018;96:1025–37.
17. Antonietti P, Gessler F, Dussmann H, Reimertz C, Mittelbronn M, Prehn JH, et al. AT-101 simultaneously triggers apoptosis and a cytoprotective type of autophagy irrespective of expression levels and the subcellular localization of Bcl-xL and Bcl-2 in MCF7 cells. Biochim Biophys Acta. 2016;1863:499–509.
18. Delgado ME, Olsson M, Lincoln FA, Zhivotovsky B, Rehm M. Determining the contributions of caspase-2, caspase-8 and effector caspases to intracellular VDVADase activities during apoptosis initiation and execution. Biochimica et Biophysica Acta (BBA) - Mol Cell Res. 2013;1833:2279–92.
19. Laussmann MA, Passante E, Dussmann H, Rauen JA, Wurstle ML, Delgado ME, et al. Proteasome inhibition can induce an autophagy-dependent apical activation of caspase-8. Cell Death Differ. 2011;18:1584–97.
20. Lindner AU, Concannon CG, Boukes GJ, Cannon MD, Llambi F, Ryan D, et al. Systems analysis of BCL2 protein family interactions establishes a model to predict responses to chemotherapy. Cancer Res. 2013;73:519–28.
21. Popgeorgiev N, Jabbour L, Gillet G. Subcellular localization and dynamics of the Bcl-2 family of proteins. Front Cell Dev Biol. 2018;6:13.
22. Imamura H, Huynh Nhat KP, Togawa H, Saito K, Iino R, Kato-Yamada Y, et al. Visualization of ATP levels inside single living cells with fluorescence resonance energy transfer-based genetically encoded indicators. Proc Natl Acad Sci USA. 2009;106:15651–6.
23. D'Orsi B, Kilbride SM, Chen G, Perez Alvarez S, Bonner HP, Pfeiffer S, et al. Bax regulates neuronal Ca2+ homeostasis. J Neurosci. 2015;35:1706–22.

24. Düssmann H, Rehm M, Kögel D, Prehn JH. Outer mitochondrial membrane permeabilization during apoptosis triggers caspase-independent mitochondrial and caspase-dependent plasma membrane potential depolarization: a single-cell analysis. J Cell Sci. 2003;116:525–36.
25. Düssmann H, Perez-Alvarez S, Anilkumar U, Papkovsky DB, Prehn JH. Single-cell time-lapse imaging of intracellular O(2) in response to metabolic inhibition and mitochondrial cytochrome-c release. Cell Death Dis. 2017;8:e2853.
26. Fercher A, O'Riordan TC, Zhdanov AV, Dmitriev RI, Papkovsky DB. Imaging of cellular oxygen and analysis of metabolic responses of mammalian cells. Methods Mol Biol. 2010;591:257–73.
27. Lucantoni F, Lindner AU, O'Donovan N, Dussmann H, Prehn JHM. Systems modeling accurately predicts responses to genotoxic agents and their synergism with BCL-2 inhibitors in triple negative breast cancer cells. Cell Death Dis. 2018;9:42.
28. Gao H, Korn JM, Ferretti S, Monahan JE, Wang Y, Singh M, et al. High-throughput screening using patient-derived tumor xenografts to predict clinical trial drug response. Nat Med. 2015;21:1318–25.
29. Oakes SR, Vaillant F, Lim E, Lee L, Breslin K, Feleppa F, et al. Sensitization of BCL-2-expressing breast tumors to chemotherapy by the BH3 mimetic ABT-737. Proc Natl Acad Sci USA. 2012;109:2766–71.
30. Vaillant F, Merino D, Lee L, Breslin K, Pal B, Ritchie ME, et al. Targeting BCL-2 with the BH3 mimetic ABT-199 in estrogen receptor-positive breast cancer. Cancer Cell. 2013;24:120–9.
31. Ashton TM, McKenna WG, Kunz-Schughart LA, Higgins GS. Oxidative phosphorylation as an emerging target in cancer therapy. Clin Cancer Res. 2018;24:2482–90.
32. Chandel NS. Mitochondria and cancer. Cancer Metab. 2014;2:8.
33. Diers AR, Broniowska KA, Chang C-F, Hogg N. Pyruvate fuels mitochondrial respiration and proliferation of breast cancer cells: effect of monocarboxylate transporter inhibition. Biochemical J. 2012;444:561–71.
34. Huang H, Hu X, Eno CO, Zhao G, Li C, White C. An interaction between Bcl-xL and the voltage-dependent anion channel (VDAC) promotes mitochondrial Ca2+ uptake. J Biol Chem. 2013;288:19870–81.
35. Shimizu S, Konishi A, Kodama T, Tsujimoto Y. BH4 domain of antiapoptotic Bcl-2 family members closes voltage-dependent anion channel and inhibits apoptotic mitochondrial changes and cell death. Proc Natl Acad Sci USA. 2000;97:3100–5.
36. Schendel SL, Montal M, Reed JC. Bcl-2 family proteins as ion-channels. Cell Death Differ. 1998;5:372–80.
37. Vander Heiden MG, Chandel NS, Williamson EK, Schumacker PT, Thompson CB. Bcl-xL regulates the membrane potential and volume homeostasis of mitochondria. Cell. 1997;91:627–37.
38. Stein LR, Imai S-i. The dynamic regulation of NAD metabolism in mitochondria. Trends Endocrinol Metab. 2012;23:420–8.
39. Bonuccelli G, De Francesco EM, de Boer R, Tanowitz HB, Lisanti MP. NADH autofluorescence, a new metabolic biomarker for cancer stem cells: Identification of Vitamin C and CAPE as natural products targeting "stemness". Oncotarget. 2017;8:20667–78.
40. Zhu L, Yu Y, Chua BH, Ho YS, Kuo TH. Regulation of sodium-calcium exchange and mitochondrial energetics by Bcl-2 in the heart of transgenic mice. J Mol Cell Cardiol. 2001;33:2135–44.
41. Imahashi K, Schneider MD, Steenbergen C, Murphy E. Transgenic expression of Bcl-2 modulates energy metabolism, prevents cytosolic acidification during ischemia, and reduces ischemia/reperfusion injury. Circ Res. 2004;95:734–41.
42. Veatch JR, McMurray MA, Nelson ZW, Gottschling DE. Mitochondrial dysfunction leads to nuclear genome instability via an iron-sulfur cluster defect. Cell. 2009;137:1247–58.
43. Geissler A, Krimmer T, Bömer U, Guiard B, Rassow J, Pfanner N. Membrane potential-driven protein import into mitochondria: the sorting sequence of cytochrome b(2) modulates the Δψ-dependence of translocation of the matrix-targeting sequence. Mol Biol Cell. 2000;11:3977–91.
44. Martinez-Reyes I, Diebold LP, Kong H, Schieber M, Huang H, Hensley CT, et al. TCA cycle and mitochondrial membrane potential are necessary for diverse biological functions. Mol Cell. 2016;61:199–209.
45. Bernal SD, Lampidis TJ, Summerhayes IC, Chen LB. Rhodamine-123 selectively reduces clonal growth of carcinoma cells in vitro. Science. 1982;218:1117–9.
46. Summerhayes IC, Lampidis TJ, Bernal SD, Nadakavukaren JJ, Nadakavukaren KK, Shepherd EL, et al. Unusual retention of rhodamine 123 by mitochondria in muscle and carcinoma cells. Proc Natl Acad Sci USA. 1982;79:5292–6.
47. Houston MA, Augenlicht LH, Heerdt BG. Stable Differences in Intrinsic Mitochondrial Membrane Potential of Tumor Cell Subpopulations Reflect Phenotypic Heterogeneity. Int J Cell Biol. 2011;2011:11.
48. Chen ZX, Pervaiz S. Bcl-2 induces pro-oxidant state by engaging mitochondrial respiration in tumor cells. Cell Death Differ. 2007;14:1617–27.
49. Geissmann Q. OpenCFU, a new free and open-source software to count cell colonies and other circular objects. PLoS ONE. 2013;8:e54072.
50. Frezza C, Cipolat S, Scorrano L. Organelle isolation: functional mitochondria from mouse liver, muscle and cultured filroblasts. Nat Protoc. 2007;2:287–95.
51. Fercher A, Borisov SM, Zhdanov AV, Klimant I, Papkovsky DB. Intracellular O2 sensing probe based on cell-penetrating phosphorescent nanoparticles. ACS Nano. 2011;5:5499–508.
52. Kondrashina AV, Dmitriev RI, Borisov SM, Klimant I, O'Brien I, Nolan YM, et al. A phosphorescent nanoparticle-based probe for sensing and imaging of (Intra)cellular oxygen in multiple detection modalities. Adv Funct Mater. 2012;22:4931–9.
53. Yang TT, Sinai P, Kain SR. An acid phosphatase assay for quantifying the growth of adherent and nonadherent cells. Anal Biochem. 1996;241:103–8.
54. Love MI, Huber W, Anders S. Moderated estimation of fold change and dispersion for RNA-seq data with DESeq2. Genome Biol. 2014;15:550.
55. Barretina J, Caponigro G, Stransky N, Venkatesan K, Margolin AA, Kim S, et al. The cancer cell line encyclopedia enables predictive modelling of anticancer drug sensitivity. Nature. 2012;483:603–7.
56. Curtis C, Shah SP, Chin SF, Turashvili G, Rueda OM, Dunning MJ, et al. The genomic and transcriptomic architecture of 2,000 breast tumours reveals novel subgroups. Nature. 2012;486:346–52.